iScience

CellPress
OPEN ACCESS

Article

Crowding induced switching of polymer translocation by the amalgamation of entropy and osmotic pressure

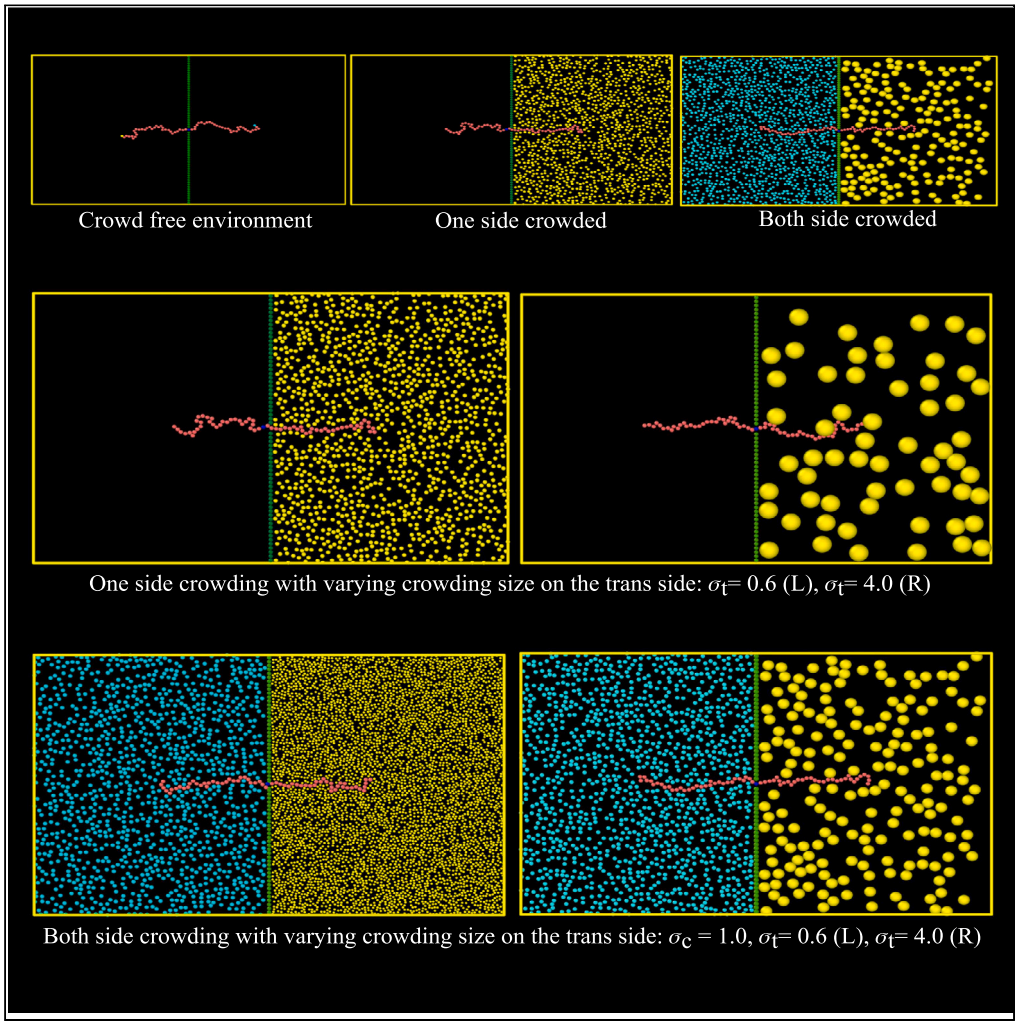

Vrinda Garg, Rejoy Mathew, Riyan Ibrahim, Kulveer Singh, Surya K. Ghosh

skghosh@nitw.ac.in

Highlights

Location-dependent translocation rate and bead velocity show counterintuitive behavior

Critical crowder size reveals non-zero translocation probability in one-sided crowding

Asymmetric polymer shift in a crowded environment overcomes the crowding effect

A slight variation in crowder size induces the polymer to switch direction

Garg et al., iScience *27*, 109348
April 19, 2024 © 2024 The Author(s).
https://doi.org/10.1016/j.isci.2024.109348

iScience

CellPress
OPEN ACCESS

Article

Crowding induced switching of polymer translocation by the amalgamation of entropy and osmotic pressure

Vrinda Garg,[1] Rejoy Mathew,[1] Riyan Ibrahim,[1] Kulveer Singh,[1] and Surya K. Ghosh[1,2,*]

SUMMARY

The translocation of polymers is omnipresent in inherently crowded biological systems. We investigate the dynamics of polymer translocation through a pore in free and crowded environments using Langevin dynamics simulation. We observed a location-dependent translocation rate of monomers showcasing counterintuitive behavior in stark contrast to the bead velocity along the polymer backbone. The free energy calculation of asymmetrically placed polymers indicates a critical number of segments to direct receiver-side translocation. For one-sided crowding, we have identified a critical crowding size revealing a nonzero probability of translocation toward the crowded-side. Moreover, we have observed that shifting the polymer toward the crowded-side compensates for one-sided crowding, yielding an equal probability akin to a crowder-free system. In two-sided crowding, a slight variation in crowder size and packing fraction induces a polymer to switch its translocation direction. These conspicuous yet counter-intuitive phenomena are rationalized by minimalistic theoretical arguments based on osmotic pressure and radial entropic forces.

INTRODUCTION

The transport of a polymer through a pore is a ubiquitous phenomenon in many biological processes and systems. Examples include RNA passing through a pore created by a membrane-bound protein,[1,2] RNA and DNA sequencing,[3–8] polymer transport processes,[9–12] gene therapy,[13–15] viral ejection,[16–19] controlled delivery,[20–22] and polymer sorting and ultrafiltration.[23] In *in vitro* setups, translocations are mainly induced by driving forces, such as external applied electric field,[18,24–29] controlling the translocation of a single molecule through a glass nanopore on a 3D nanopositioner,[30,31] pulling force exerted on polymer's end,[32–34] binding particles (chaperones),[35–38] are known as forced translocation.[39] In many biological systems, unforced translocations occur naturally dictated by conformational entropy.[16,18,40,41] Despite its omnipresence and importance in biological processes, unforced translocation has received less attention.[40,41] Especially the system's intrinsic parameters, such as the symmetry of the length distribution of the polymer being translocated and the effects of crowding present in the cellular environment. Here, we investigate the generic behavior of self-avoiding flexible polymers[42] exhibiting unforced translocation through a pore for free and crowded environments. A deeper understanding of these natural unforced processes can help in designing more efficient practical *in vitro* setups.

Polymer translocation through pores displays a broad range of scaling regimes, as shown by numerical simulations,[43–46] analytical theories,[47,48] and experiments.[18] The average translocation time τ as a function of the chain length N is an important measure of the underlying dynamics. Especially in the case of unforced translocation, the barrier is so high that it is almost practically impossible to have a successful translocation solely due to the thermal agitation for long polymer chains in the limit of $N \gg 1$.[32] As the repeated chemical units of the polymer pass through the pore, they encounter a depletion in their available conformational entropy creating an overall entropic barrier resulting in constrained diffusion. According to Kramers' analysis of diffusion across an entropic barrier, the translocation time is scaled as $\tau \sim N^{\alpha}$, for phantom chains in the case of unforced translocation the scaling exponent is $\alpha = 2$ ($\tau \sim N^2$) and for the forced translocation $\alpha = 1$ ($\tau \sim N$).[49] The Rouse model for the dynamics of phantom chains also predicts a time of the order of N^2 for equilibration. For a phantom chain, translocation time depends on the relative magnitudes of three-time scales in terms of dimensionless factor that characterizes the translocation process $\tilde{\tau}$ and medium's viscosity η: total translocation time $\tau \sim (b^2/D_p)\tilde{\tau}$, polymer relaxation time $\tau_R \sim (\eta b^3/k_BT)N^2$, and $\tau_0 \sim \varphi^{-2/3}/D_0$ for obstacles motion, where Gaussian polymer (phantom chain) of length N (in units of the Kuhn length b) has diffusion coefficient D_p, D_0 is the diffusion coefficient of obstacles, and φ is the volume fraction of randomly distributed obstacles. Two regimes exist depending on the relative mobility of the obstacles: the dynamic obstacles regime where $\tau_0 \ll \tau_R \ll \tau$ and the static obstacles regime where $\tau_R \ll \tau \ll \tau_0$.[14,15,32,40,47,50,51] With excluded volume, in the presence of an external driving force f, the translocation time τ scales as $\tau \sim N^{\beta}/f^{\gamma}$ where γ is the scaling

[1]Department of Physics, National Institute of Technology, Warangal 506004, India
[2]Lead contact
*Correspondence: skghosh@nitw.ac.in
https://doi.org/10.1016/j.isci.2024.109348

This is an open access article under the CC BY-NC license (http://creativecommons.org/licenses/by-nc/4.0/).

exponent associated with the external forces. Biased translocation exhibits anomalous behavior with various values of both these exponents in several experimental[52,53] and computational studies.[54,55] Once self-avoidance is included, translocation time increases dramatically with a scale of $\alpha = 2.5$ ($\tau \sim N^{2.5}$), which is an exponent of Rouse relaxation of self-avoiding chain in 2D.[32,54] For the self-avoiding chain, the translocation time is longer than the Rouse relaxation time ($\tau \gg \tau_R$). According to the Flory-exponent theory, the scaling of translocation time for a self-avoiding chain is given as $\tau \sim N^{\beta}$ where $\beta = 1 + 2\nu$ and with the flory exponent $\nu = 0.75$ ($\tau \sim N^{2.5}$) in 2D and $\nu = 0.588$ ($\tau \sim N^{2.176}$) in 3D.[36,50,51] Likewise, the scaling for MSD has been noted. It takes the power law form: $\langle \Delta r^2(t) \rangle \sim t^{\alpha}$, where α is the anomalous diffusion exponent. It is observed that $\alpha = 0.8$ resembles the experimental value.[40,54,56] The shapes and sizes of the fluidic channel and cavity[57] also have a strong effect when a polymer is translocated into or out of a confined environment.[26,43,51,58]

In this work, we considered a self-avoiding flexible polymer in an unbiased and unforced environment, threading its way through the pore as a fundamental model and as a first step toward understanding the translocation dynamics *in vivo* set-ups. Here, we specifically focused on the system's intrinsic parameters rather than the external influences. We examined certain parameters to elucidate translocation dynamics in this system thoroughly. Quantitative measurements of the probability of translocation events and the corresponding translocation times through the pore provide a fundamental basis for our study and validate the process. To understand the diffusion mechanism, we investigate the MSD of the center of mass of polymer, head, middle, and tail monomers. A study on how different segments of the polymer are moving across the pore is drawn to attention. We examine the quantities, such as the average bead crossing time of individual monomers, the translocation rate of each bead, and their translocation speed across the pore. In particular, we find a counterintuitive trend of monomers' translocation rate and translocation speed as they pass through the pore.

As the polymer translocates through the pore, the number of accessible conformations significantly reduces. This leads to a decrease in the chain's conformational entropy and an increase in its free energy. We examined the free energy profile for the no-crowding case and observed a symmetric free energy barrier when the polymer chain is placed symmetrically at the pore. This analysis resembles the analytical calculations.[59] Further, we find that an asymmetrically placed polymer leads to a critical number of segments that, when translocated, causes the free energy minima and polymer to prefer the receiver side.

The highly crowded environment of actual biological cells containing large macromolecules like proteins, lipids, ribosomes, and cytoskeleton fibers features volume occupancies up to $\varphi \sim 40\%$. Studying the impact of crowding is crucial for comprehending translocation in realistic cellular environments due to high cell density.[47,57,59,60] A number of recent works have shed light on the translocation processes in the presence of non-inert crowder (chaperons).[35,38] An aspect that has received very little attention is the impact of inert crowding, resulting in a biased but still unforced system by introducing crowders at one side of the box, leading to asymmetric crowding and on both sides of the box, creating a symmetric crowded environment as a second step to understand the translocation dynamics in crowded *in vivo* set-ups. Polymer threading its way through such an environment is subjected to an entropic penalty, and interaction between crowder-polymer affects the translocation dynamics. Here, we quantify the effects of modifying the length distribution of polymer from its initial configuration, varying the size and packing fraction of the crowders, and show that it significantly affects the translocation dynamics. We find that when the crowders size reaches a crossover and deviates from the size of each chemical unit of the polymer, the polymer-crowder interaction fundamentally changes the direction of translocation and shows a sudden jump within two extremes of probability. Moreover, we show that by tuning the crowded environment, we can control the dynamics and switch the direction of the translocation process, which can be applied for better drug delivery, DNA sequencing, and transport processes.

The article is constructed as follows: In first section, we present the simulation results and discussions for the three distinct modeling frameworks. Firstly, we examine the dynamics of polymer translocation without crowder. Next, we investigate the impact of the crowder on one side of the box. Finally, we study the translocation process driven by the crowders on both sides of the box. Followed by the section which summarizes the conclusions drawn from this work. In the end, we elucidate the methods and models employed in this study.

RESULTS

Translocation without crowders

Translocation probability (P), time (τ), and MSD

We first considered the polymer translocation in a crowd-free medium (Figure 1A and Video S1). We calculated the translocation probability P and time τ. The translocation probability P can be defined as the ratio of successful translocation events toward a particular side to the total number of successful events.[36,40] The probability of the polymer to translocate to *cis* (left) side is represented by P_c and to the *trans* (right) side is P_t. The time required for a polymer positioned symmetrically with a center bead initially at $t = 0$ in the middle of the pore to fully translocate to either side of the wall is referred to as translocation time τ. If the polymer goes to the *cis* (left) side, we call it a *cis*-translocation time τ_c, and for *trans* (right) side, it is a *trans*-translocation time τ_t.

Ideally, in the absence of crowders (Figure 1A), the system remains unbiased from either side and exhibits an equal probability of translocation.[40] As expected, from our model, we have observed equal *cis* and *trans* translocation probability, $P_c \approx P_t \approx 0.5$, for different polymer length N (Figure 2A). The translocation time τ scales as $\tau_c \sim \tau_t \sim N^{2.5}$ (Figure 2B), as we vary length N, exactly matches with analytical and previously found simulation studies on unforced free polymer translocation.[47,54]

To understand the dynamic behavior of the polymer, we analyzed the time evolution of mean squared displacement (MSD(t)) of the center of mass $g_3(t)$ and individual monomers: the first monomer $g_{head}(t)$ for $s = 1$, mid monomer $g_{mid}(t)$ for $s = N/2 + 1$, and end monomer $g_{tail}(t)$ for $s = N + 1$. In general, the MSD(t) takes the following power law form: $\langle \Delta r^2(t) \rangle \sim t^{\alpha}$, where α is the anomalous diffusion exponent. Each danging end outside the pore has a characteristic relaxation time τ_R much faster than that of the monomer moving through the pore. The

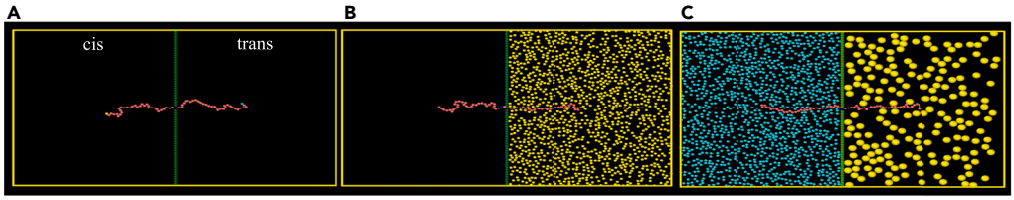

Figure 1. Polymer translocation in free and crowded environment

Schematic illustration of polymer translocation process through a pore. The wall in the middle of the box consists of purely repulsive immobile LJ particles of size σ the same as the size of each monomer. Here, we show the initial configuration of all the systems with a flexible polymer being symmetrically placed at the pore. The left part of the system represents the *cis*-side and the right part of the system is *the trans*-side. In this schematic, we have used a polymer of length $N = 65$.

(A) In a crowd-free environment.

(B) In the presence of one-sided crowding where yellow particles represent the crowders on the *trans* side.

(C) When crowders are present on both sides. Here, bigger crowders are shown in yellow and smaller crowders in blue. Packing fractions of crowders on both sides is kept the same. We are changing the size of the crowders on the *trans* side, keeping the size of the crowders on *cis* side fixed.

relaxation time (Rouse time) τ_R of a polymer is typically defined as the characteristic time it takes to diffuse a distance of the order of its size.[61] At small time scales when time t is much less than the relaxation time τ_R ($t < \tau_R$), the movement of the individual monomers is different from the center of mass movement, resulting in a significant difference in their $MSD(t)$. At a later time, when t is greater than relaxation time τ_R ($t > \tau_R$), the MSDs of the middle monomer coincide with the center of mass. For the translocation of a self-avoiding chain in 2D, the exponent can be written as $\alpha = 2/(1+2\nu)$ where ν is the flory swelling exponent. In the long time limit, the $g_{mid}(t)$ and $g_3(t)$ converge with $\alpha = 0.8$ for $\nu = 0.75$ (Figure 2C).[40,54] Moreover $g_{head}(t)$ and $g_{tail}(t)$ also show similar behavior with exponent $\alpha = 0.8$. However, as the two ends of the polymer danging in bulk with more translational degree of freedom, the MSD values are always greater than the other or center of mass monomers.

Translocation rate, crossing time, and, bead velocity

During translocation processes, it is observed that different segments of the polymer move differently. To envision this interesting phenomenon, we calculated the average bead crossing time $\tau_{crossing}$, translocation rate k_T, and bead velocity $v_i(t)$ for different segments of the polymer. Our focus centers on investigating and highlighting the translocation rate and bead velocity of an individual monomer, excluding considerations for the polymer as a whole.

The average time taken by a monomer to translocate through the pore is defined as the average bead crossing time $\tau_{crossing}$. Figure 3A shows the variation in crossing time taken by each monomer to pass the pore starting from their respective initial position in bulk. As expected, for different monomers, as we move along the backbone of the chain, the crossing times are different. Due to the closeness of the pore, the central monomers take a shorter time to pass the pore over their faraway peers, the tail monomers. In spite of this trivial realization, if we look closely, we can observe that the rate of change of $\langle\tau_{crossing}\rangle$ with respect to monomer id is not constant but rather increases as it moves toward the tail. This interesting feature will be addressed during the discussion of k_T in the following section.

The translocation rate k_T is defined as the number of beads passing through the pore per unit time. k_T is calculated by taking the derivative of the curve in Figure 3A. As the translocation process starts with the center bead $(N-1)/2$ at the pore, the translocation rate increases slowly for beads near the center of the polymer chain due to alike entropic force from both sides. The small values of k_T in the middle clearly indicate that during the translocation event, the monomers in the middle region have several back-and-forth movements around the pore before they fully translocate to one side. Subsequently, once the translocation of some significant middle portion of the polymer has taken place,

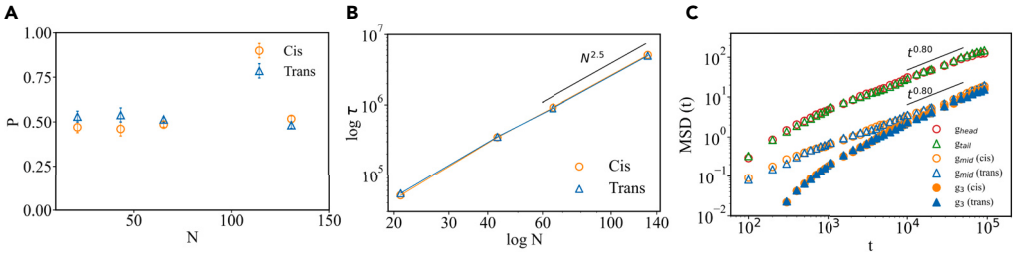

Figure 2. Translocation probability (*P*), time (τ), and MSD

(A) Translocation probability P of free polymers of different lengths: $N = 21, 43, 65,$ and 131. Translocation probability to *cis*-side is shown by circle and to the *trans*-side by triangle.

(B) Scaling of the translocation time τ with respect to the polymer of length N for no crowding case. As expected, average τ shows the same behavior in the case of *cis* and *trans* translocation for varying lengths of polymer with the scaling of $\tau_c \sim \tau_t \sim N^{2.5}$.

(C) The mean-squared displacement MSD(t) of the first monomer $g_{head}(t)$, middle monomer $g_{mid}(t)$, end monomer $g_{tail}(t)$, and center of mass $g_3(t)$ of the polymer of $N = 65$. Here, we obsrved that the plot shows alike behavior for both sides, giving expected value of $\alpha = 0.8$ at long times.

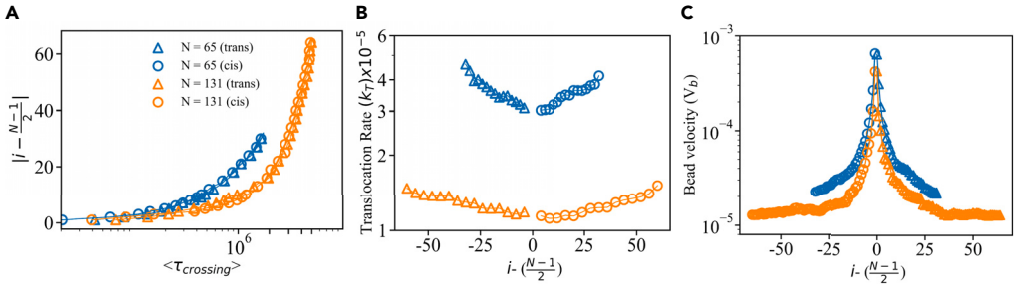

Figure 3. Translocation dynamics of individual bead through a pore, bead crossing time ($\tau_{crossing}$) of the individual monomer, translocation rate (k_T), and bead velocity (V_b)

(A) For a polymer chain of N monomers labeled $i = 1, 2, 3, \cdots, N$ having center at $(N-1)/2$, its left-side can be represented as $j_L = i, 1 \leq i < (N-1)/2$ and right-side of the chain as $j_R = (N-1)/2 - i, (N-1)/2 \leq i \leq N$. Monomer id with respect to the center bead $(N-1)/2$ of the polymer against average bead crossing time $\tau_{crossing}$ of polymer length $N = 65$ (blue), 131 (orange) is plotted.

(B) Translocation rate k_T of polymer of length $N = 65, 131$. The graph is plotted symmetrically with respect to the center bead at the pore. Curves on the left represent the translocation rate of j_L to show *trans*-translocation (triangles), and the right curve represents the translocation rate of j_R to show *cis*-translocation (circle).

(C) Bead velocity v_b of the individual monomer for polymer of length $N = 65, 131$. The figure is plotted symmetrically with respect to center bead ($(N-1)/2$) at the pore and indicates bead velocity when moving to the *trans*-side (triangle) and *cis*-side (circle).

follow-up monomers motion is governed by the already translocated part, leading to a higher translocation rate for the tail monomers (Figure 3B). The ratio of the translocation rates of the center monomer with respect to the polymer end monomer are defined as $\overline{k}_L = k_T(n_{first})/k_T(n_{center})$ for the *cis*-side, $\overline{k}_R = k_T(n_{end})/k_T(n_{center})$ for the *trans*-side, and the average of the ratio of translocation rate $\langle k_0 \rangle = (\overline{k}_L + \overline{k}_R)/2$. The average of the ratio of the translocation rates, $\langle k_0 \rangle$, for the initial and end monomers on the cis ($\overline{k}_L$) and trans ($\overline{k}_R$) sides relative to the central monomer exhibit almost similar ratios of approximately 1.4 and 1.3 for lengths $N = 65, 131$, respectively (see Table 1).

Now let us look at the individual bead velocity $v_i(t) = dr_i(t)/dt$, which tracks the dynamics of the movement of the i^{th} bead during a translocation process. We have observed that middle monomers move faster than tail monomers (Figure 2C). Being close to the pore, the monomers in the central region are restricted to exhibit quasi-one-dimensional diffusion from the beginning of the translocation process until a successful crossover of that bead happens. While for most of the translocation time, the tail monomers undergo 2D diffusion until they approach the vicinity of the pore, resulting in lower $v(t)$. From the MSD Study in Figure 2C and bead velocity in Figure 3C, it can be observed that initially, the dangling tail monomers wander in the medium for a reasonable amount of time and diffuses slowly. In contrast, the middle monomers in the vicinity of the pore, part of quasi-one-dimensional diffusion, diffuses faster, supporting the notion that resulted in higher $v(t)$ for middle monomers than the tail monomers during the translocation process.[55,62] The monomer velocity dramatically increases when it approaches the vicinity of the pore.

Asymmetrically placed polymer

Until now, in the free environment, we have studied translocation by always placing the polymer symmetrically between the cis and trans side, with the middle monomer at the pore as the initial configuration. Now, we are breaking the symmetry by asymmetrically placing the polymer from its middle with extra length into the trans side. As a result, we are designing the initial configuration so that when the translocation process starts, the polymer portion on the trans side is larger than the cis side. We want to know what the free energy of the chain is as the polymer translocates from one region to another see Figure S1 and Video S2. We are interested in examining the impact of the asymmetrically placed polymer on translocation probability see Figure 4. When a polymer translocates through the pore, the chain goes through a decrease in its conformational entropy, and the excluded volume interactions become more pronounced, increasing the free energy of the chain. Here, pore size is assumed to be short in comparison with the length of polymer molecules that can be considered as a small hole in an infinite wall and can allow only one monomer to pass through at a time.[13,15,40,63] The two translocating polymer segments on the cis and trans side can be treated as two thermodynamic ensembles separated by the wall. At any state, let there be n segments of the translocating polymer in the *trans*-side referred to as *receiver* and $N - n$ segments in the *cis*-side as *donor*, both are in separate thermal equilibrium. The terms "donor" and "receiver" designate the sides for polymer translocation, with the donor being where the polymer originates and the receiver being the target (translocated) side. In our study, we named the cis side as the donor and the trans side as the receiver for clarity. In the context of observing free crowders, side nomenclature can be chosen for

Table 1. The ratio of translocation rate of the end bead on the *cis*-side and *trans*-side with respect to the center bead is given by $\overline{k}_L$ and $\overline{k}_R$ respectively

N	$\overline{k}_L$	$\overline{k}_R$	$\langle k_0 \rangle$
65	1.37	1.49	~ 1.4
131	1.32	1.25	~ 1.3

The average of the ratio of translocation rate, $\langle k_0 \rangle$, is the mean of $\overline{k}_L$ and $\overline{k}_R$. We observe a similar values of $\langle k_0 \rangle$ for different polymer lengths N.

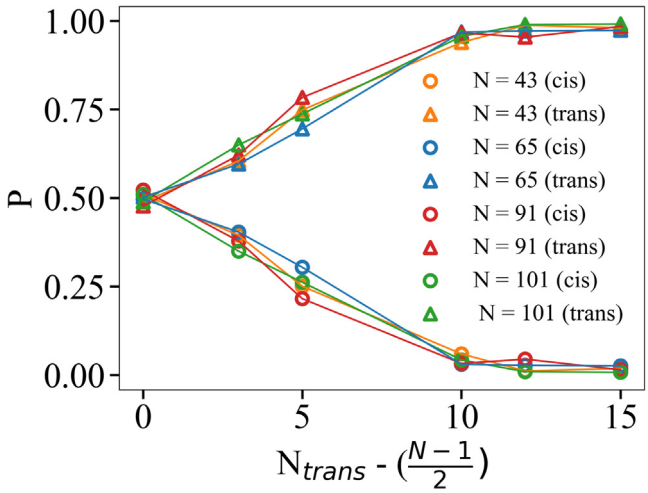

Figure 4. Effect of asymmetrically placed polymer on nucleation barrier

Plot of probability of translocation (P) vs. the number of monomers being shifted to the trans side. Here, N_{trans} is the length of the polymer on the trans side, and $(N-1)/2$ represents the middle of the polymer length N. The probability of overcoming the nucleation barrier for further successful translocation for asymmetrically placed polymer toward the *trans*-side is plotted. Asymmetry introduced in the polymer, which was initially placed symmetrically at the pore, is represented in terms of the number of monomers shifted from its middle to the trans side and shown as $N_{trans} - (N-1)/2$. For symmetrically placed polymer, $N_{trans} - (N-1)/2 = 0$, which gives $N_{trans} = (N-1)/2$. The probability of *cis*-side (circle) and *trans*-side (triangle) for the different N is shown. It starts from $P = 0.5$ for the symmetrically placed polymer when $N_{trans} = (N-1)/2$ and reaches saturation when a sufficient amount of monomers has been shifted for the nucleation phenomenon.

convenience. The partition sum Z consisting of the total number of conformations of the chain can be written as $Z = Z_d(N-n)Z_r(n)$. The partition sum $Z(N)$ for a long tail $N \gg 1$ of N segments in the semi-infinite space (half) bounded by an impenetrable wall to which one end is anchored is given as $Z_{half}(N) = \bar{z}^N N^{\gamma-1}$ where $\bar{z}$ is the effective coordination number for the orientation of adjacent bonds and is commonly known as the connective constant. It can be alternatively written as $\exp(-\mu/k_BT)$, where μ is the chemical potential per segment. γ is the critical exponent and depends on the nature of the polymer and the solution. To mimic a good solution condition for a self-avoiding polymeric chain, we have $\gamma = 0.69$. The Helmholtz free energy is $F_{half}(N) = -k_BTlnZ_{half}(N)$, elaboratively can be written as $\frac{F_{half}(N)}{k_BT} = \frac{\mu N}{k_BT} + (1-\gamma)\ln N$. The logarithmic part plays a significant role in establishing a free energy profile for polymer translocation. The total free energy of the chain $F(n)$, with n segments translocated into the *receiver*-side can be written as the sum of free energies of the two tails,

$$\frac{F(n)}{k_BT} = (1-\gamma_d)\ln(N-n) + (1-\gamma_r)\ln(n) - \frac{n\Delta\mu}{k_BT}, \qquad \text{(Equation 1)}$$

where γ_d and γ_r are critical exponents in donor and receiver region respectively. $\Delta\mu = \mu_d - \mu_r$, where μ_d and μ_r are the chemical potentials of the polymer segments in the donor and receiver region respectively. The first two terms on the RHS emerged from the entropy of two tails and clearly resulted in the free energy barrier. In general, for this free energy barrier with its maximum value F^*, there exists a critical number of translocated segments to *receiver* side, that is, n^* which can be obtained as the solution of $\partial F(n)/\partial n = 0$, gives

$$\frac{n^*}{N} = \frac{(\tilde{\mu}+2-\gamma_d-\gamma_r)}{2\tilde{\mu}} - \frac{\sqrt{(\tilde{\mu}+2-\gamma_d-\gamma_r)^2 - 4\tilde{\mu}(1-\gamma_r)}}{2\tilde{\mu}}, \qquad \text{(Equation 2)}$$

where $\tilde{\mu} = N\Delta\mu/k_BT$. For the crowd-free case, the critical value of n^* can be obtained by putting $\Delta\mu = 0$ in Equation 1. In our model, we are taking $\gamma_d = \gamma_r = \gamma$. Then, Equation 1 can be written as

$$\frac{F(n)}{k_BT} = (1-\gamma)\ln[n(N-n)]. \qquad \text{(Equation 3)}$$

The critical number of translocated segments to *receiver* side n^* for F^* is

$$\frac{\partial F(n)}{\partial n} = \frac{(1-\gamma)(N-2n)}{n(N-n)}, \qquad \text{(Equation 4)}$$

solution of $\partial F(n)/\partial n = 0$ gives $n^* = N/2$. Figure 5A shows $F(n)$ vs. n, which represents the free energy landscape of polymer translocation in the crowd-free case as a function of the translocation extent. This can be interpreted as when there is a slight deviation from the maxima of F^* at $n^* = N/2$, the free energy landscape is downhill on both sides (Figure 5A). The free energy barrier is symmetric when a polymer is symmetrically placed in its middle at the pore. Polymer tends to minimize its energy and is favorable to translocate to either side. In general, the presence of n^*

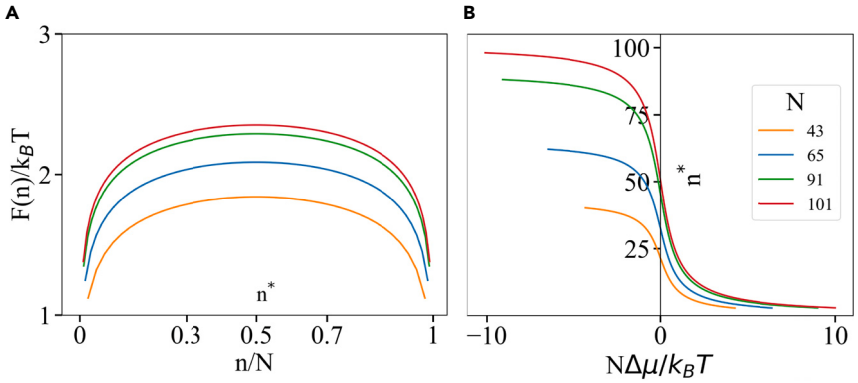

Figure 5. Analysis of Free energy and critical number of polymer segments in translocation process

(A) Plot of Free energy $F(n)$ vs. n/N, where n represents the number of asymmetrically shifted segments towards the trans side, and N is the polymer length. Here, n can varies from the initial monomer of the polymer chain to its entire length. n^* is the critical number of polymer segments representing the free energy maxima. (B) Change in n* against $N\Delta\mu$. Plot showing the dependence of the critical number of polymer segments translocated on the trans side n^* on $N\Delta\mu/\ k_BT$ for the polymer of different lengths $N = 43,65,91,101$. When $\Delta\mu = 0$, which leads to $n^* = N/2$ as we move toward the positive side, n* decreases rapidly. This plot considers two sides of the wall: the receiver and the donor. The chemical gradient is calculated from the difference between the donor and receiving side, and the sign decides the direction in which translocation could be preferred. For the case of one-sided crowding where the crowders reside on the receiver side, and $\varphi_{donor} = 0$ gives $\Delta\mu = \mu_{donor} - \mu_{receiver} = 0 - \mu$, where μ is a positive quantity and the polymer tends to move to the free *cis* (donor) side. For the case of both-sided crowding, the sign of $\Delta\mu$ depends on the difference of crowding concentration on the donor and receiver side.

indicates that translocation resembles a nucleation phenomenon.[63] If the number of segments is less than n^*, then segments still tend to return to *donor* side. The translocation process is stochastic, like a nucleation phenomenon. Once a sufficient number of monomers have crossed the nucleation barrier to the *receiver* side and are larger than n^*, translocation to this side is more favorable as the free-energy profile is now downhill. Hence, a critical number of n^* ought to be nucleated in the *receiver* side to make translocation successful. The variation of free energy $F(n)$ with the entire length of the polymer with its critical points represented with circles is shown in Figure S4. This free energy curve is helpful in understanding Figure 4. In this plot, the probability of overcoming the nucleation barrier for further successful translocation for asymmetrically placed polymer vs. the number of monomers being shifted to the trans side is plotted. Here, N_{trans} is the length of the polymer on the trans side, and $(N-1)/2$ represents the middle of the polymer N. Asymmetry introduced in the polymer, which was initially placed symmetrically at the pore, is represented in terms of the number of monomers shifted from its middle to the trans side and shown as $N_{trans} - (N-1)/2$. From the probability plot, it can be seen that as soon as we start placing the polymer asymmetrically on the trans side, that is when it deviates from $N_{trans} - (N-1)/2 = 0$, which gives $N_{trans} = (N-1)/2$ symmetrically placed polymer, it starts preferring the trans (receiver) side. Once a significant section of the polymer is shifted to the trans (receiver) side (say approximately 60% of the length) and once the nucleation barrier is crossed, the polymer slowly reaches a free-energy minima and it can undergo further translocation to receiver side without coming back to the donor side. In Figure 6 we construct phase plots for n^*/N in the $\Delta\mu - N$ plane. The effect of the chemical potential gradient can be seen in Figure 6. For a crowd-free environment, $\Delta\mu = 0$, n^*/N is exactly half for all chain lengths N, and the free energy barrier is symmetric, shown by the black dotted line in Figure 6. Another situation is translocation into a crowded environment driven by a chemical potential gradient. For the case of one side crowding where the trans side has crowders having $\varphi_c = 0$ and $\Delta\mu = \mu_{cis} - \mu_{trans} = 0 - \mu = -\mu$, where μ is a positive quantity and the polymer tends to move to the free cis side. However, a critical value of polymer segment n^* can reverse this trend, which is sufficient to overcome the osmotic pressure. See the upper panel of Figures 5B and 6. The free energy barrier is bigger when the chemical potential gradient $\Delta\mu = -\mu$ is in the opposite direction to the translocation process. Since the barrier is bigger despite being crossed, the chain in the receiver region remains in a metastable state and will eventually tend to revert to the donor region. For this case, a higher value of n^*/N is needed for a favorable translocation in the receiver region. For lower pannel of Figure 6 and large values of N and $\Delta\mu$, n^* becomes progressively small. We require only a small segment of the polymer to be shifted at the cost of chemical potentials, such as for $N = 100$, $\Delta\mu = 0.01$, it can be compensated by $n^* = 22$ for the nucleation process to happen.[59] In our model of polymer translocating through the crowd-free environment, we have observed that nucleation phenomenas start at $n^* = 10$ (Figure S5). The dependence of Free energy maxima F^* on the chain length N and chemical potential gradient $\Delta\mu$ has been given in (Figure S6). In Figure 5B, we can see a sudden drop in the curve when $\Delta\mu$ deviates from zero. As soon as the crowding is introduced, starting from the small size of the crowders, there is a critical value of σ for a change in $\Delta\mu$ at which the polymer chain will face energy downhill with respect to n. This trend can be seen in the one-sided crowding case (Figure 7). For small σ_c we have a high value of $\Delta\mu$, crowding has a strong effect on pushing the polymer to the crowd-free side and resulting in a sudden rise which gives $P_c = 1$. While the case of higher σ_c and comparatively lower $\Delta\mu$ will create larger voids in the crowding side. The polymer still has a small but non-zero P_c. This would suggest the critical point where the translocation can act as the nucleation phenomenon, with few monomers passing through the pore. Very less shifting of polymer, even with the small value of n, will escalate the translocation to the crowded side. A detailed discussion of the effect of one-sided (*trans*) crowders on the translocation probability is done in the next section. The dependence of this critical number $n*$ per unit length N with changing $\Delta\mu$ has been given in (Figure S7).

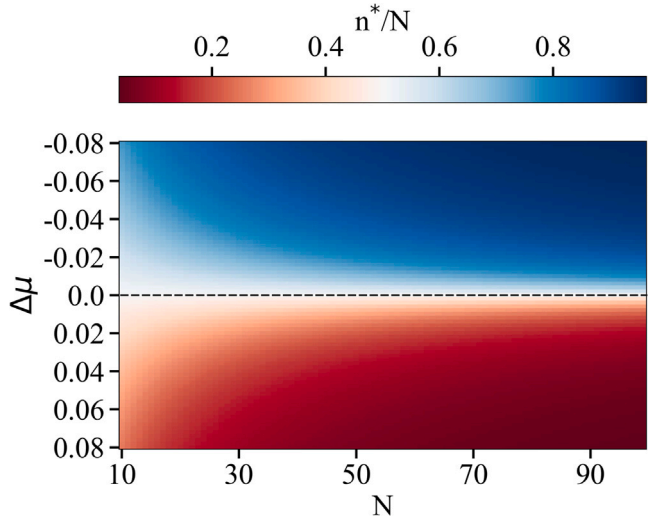

Figure 6. Phase plot of n^*/N in $\Delta\mu$-N plane

Here, n^* is the critical number of polymer segments into the trans side. The existence of free energy maxima at n^* tells that translocation is like a nucleation phenomenon, i.e., n^* critical number of segments are to be nucleated for translocation to be successful. N is polymer length and $\Delta\mu$ is the chemical potential gradient between *cis* and *trans*-side. The black dashed line represents no crowding case where $\Delta\mu = 0$ and n^*/N is exactly half for all chain lengths N, and the free energy barrier is symmetric. The chemical potential gradient varies from negative to positive, shown by blue to red.

Effect of one-side crowders

We now study the impact of one-sided inert crowders on the translocation process (Figure 1B and Video S3). The study of inert crowders on both sides[50] and non-inert crowders on one side (chaperones)[38] has been studied. However, a detailed investigation of translocation processes with inert crowders on one side did not get its due attention. For this purpose, we choose to put inert crowders only on one side,

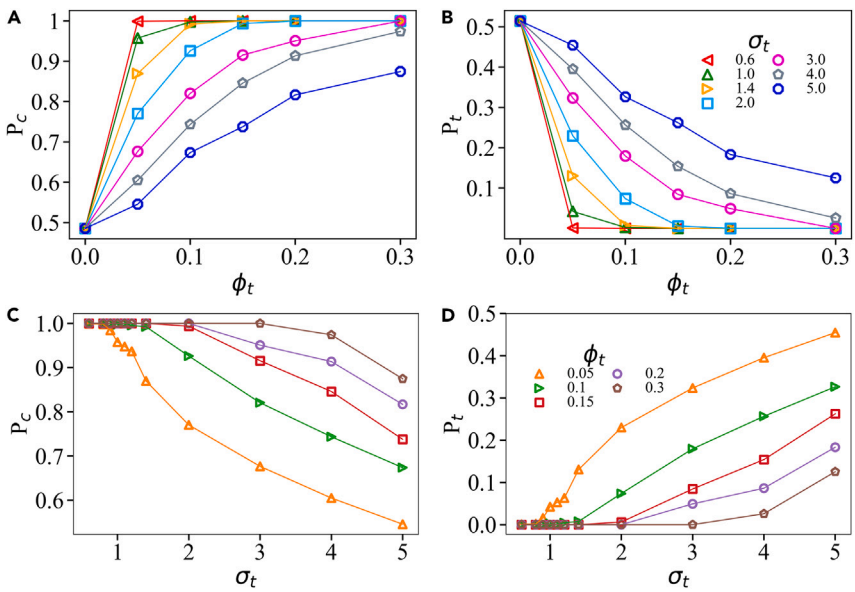

Figure 7. Translocation probability as a function of φ_t, σ_t

Upper panel: Translocation probability as a function of packing fraction of inert crowders on the *trans* side φ_t.

(A) Translocation probability P_c to *cis*-side vs φ_t for different σ_t.

(B) Translocation probability P_t to *trans*-side vs φ_t for different σ_t.

Lower Panel: Translocation probability as a function of σ_t of inert crowders on the *trans* side.

(C) Translocation probability P_c to *cis*-side vs σ_t for different φ_t.

(D) Translocation probability P_t to *trans*-side vs σ_t for different φ_t.

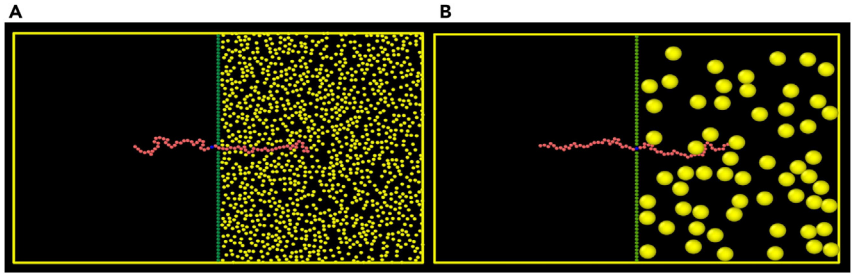

Figure 8. Translocation dynamics in the presence of crowders in one-side (trans)

Schematic illustration of translocation process of a polymer in the presence of crowder on the trans side.

(A) The packing fraction of the crowder on the trans side is $\varphi_t = 0.3$ for $\sigma_t = 0.6$ (case: $\sigma_t < 1$).

(B) For the trans side is $\varphi_t = 0.3$ for $\sigma_t = 4$ (case: $\sigma_t > 1$).

say the *trans* side, in our case (Figure 8) and studied the translocation phenomena of a symmetrically placed flexible polymer. As expected, we have observed that the translocation probability and time have a strong dependency on the packing fraction φ_t and crowding size σ_t. To understand the underlying mechanism of this effect, we first quantify the ballpark average distance between the crowders $\langle r_s \rangle$ and mean entropic force $\langle F_r \rangle$. Consider N_t is the total number of crowders on the *trans*-side, each with size, σ_t.[50] The packing fraction on the *trans*-side, with dimension $L_x \times L_y$ is

$$\varphi = \frac{N_t \pi \left(\frac{\sigma_t}{2}\right)^2}{L_x \times L_y}. \quad \text{(Equation 5)}$$

Note that the dimension of the box is $2L_x \times L_y$. Now for a fixed φ, the average distance between crowders, taken from their center $\langle r_c \rangle$ can be written as,

$$\langle r_c \rangle = \frac{\sqrt{L_x \times L_y}}{\sqrt{N_t}}. \quad \text{(Equation 6)}$$

Hence, the average distance between the surface of crowders $\langle r_s \rangle$ is

$$\langle r_s \rangle = \langle r_c \rangle - \sigma_t = \frac{\sqrt{L_x \times L_y}}{\sqrt{N_t}} - \sigma_t. \quad \text{(Equation 7)}$$

For the box of the same dimension, inserting the value Equation 5 in the Equation 7, we get

$$\langle r_s \rangle = \sigma_t \left(\frac{1}{2} \sqrt{\pi/\varphi} - 1 \right). \quad \text{(Equation 8)}$$

From the above expression we observed that the average distance between the surface of the crowders $\langle r_s \rangle$, that is the space available for the polymer to explore, is proportional to the crowder size, $\langle r_s \rangle \propto \sigma_t$, and inversely proportional to the square-root of the packing fraction, $\langle r_s \rangle \propto 1/\sqrt{\varphi}$. This behavior plays a crucial role in understanding the effect of crowders on translocation. A detailed explanation of its significance can be found in the coming section of translocation probability. The focus of our study is on the regime of packing fraction of crowder $\varphi < 0.5$. According to the percolation theory, the fluid phase is considered continuous,[64,65] indicating the formation of channels by crowders. Now, we consider average radial entropic force $\langle F_r \rangle$ and its role in the translocation process.[66,67] Radial entropic force describes the force exerted on a monomer by the particles as it moves through the channel formed by the crowders and drives the polymer to translocate through the pore. It is proportional to the temperature, inversely proportional to the confinement created by the crowders, and equivalent to inter-crowders separation.[50,68] Mean radial entropic force can be written as

$$\langle F_r \rangle = F_0 \frac{k_B T}{\langle r_s \rangle}, \quad \text{(Equation 9)}$$

where k_B is the Boltzmann constant, T is the absolute temperature, and F_0 is the proportionality constant depends on the solvent-polymer interactions. Simplifying the expression in the terms of σ, φ, we have

$$\langle F_r \rangle = F_0 \frac{k_B T}{\sigma_t \left(\frac{1}{2} \sqrt{\pi/\varphi} - 1 \right)} \quad \text{(Equation 10)}$$

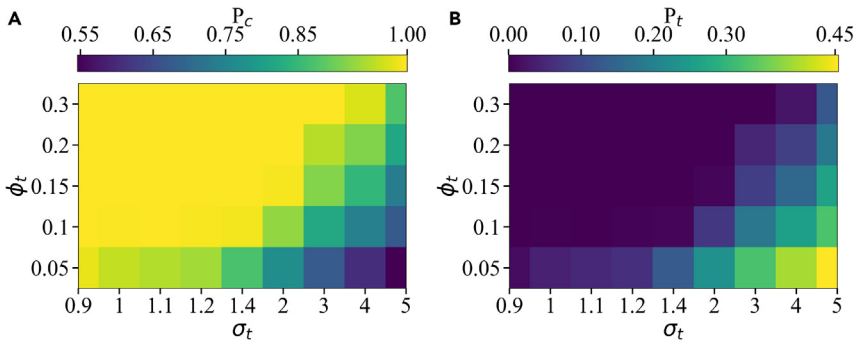

Figure 9. Phase plot of translocation probability in $\varphi_t - \sigma_t$ plane

The plot elucidates how translocation probabilities P_c and P_t vary as the function of the size of crowders (σ_t) and their packing fraction (φ_t) in one-sided *(trans)* crowded environment.

(A) Translocation probability P_c to the free-side *(cis)*.

(B) Translocation probability P_t to the crowded side *(trans)*.

The presence of crowders on the *trans*-side restricts the motion of the polymer and reduces its possible configurational entropy, which in turn reduces the entropic force acting on the polymer. This resulted in a lower entropic state in the *trans*-side compared to the *cis*-side, which has no crowders and, therefore, less restriction on the polymer's motion. The difference in entropy between the two sides serves as a driving force for the polymer to translocate from the lower entropy (*trans* side) to the higher entropy (*cis* side).[50] To elucidate the dynamics of polymer translocation through a crowded environment driven by different sizes, we examine the role of osmotic pressure (Π). Being a colligative property, *osmotic* pressure is proportional to the solute concentration ρ_c, and temperature T, can be written as $\Pi = R\rho_c T$, where R is the constant of proportionality. It can be used to determine the direction of polymer movement through the pore in response to the difference in crowding concentration gradient on either side.[14,59,69] The polymer is influenced by this osmotic pressure difference, which drives it to the *cis*-side where the concentration and, hence, pressure are lower and have more free volume. The entropic force also pulls the polymer in the direction of higher entropy, which is toward the *cis*-side. The interplay between these two forces determines the overall direction of polymer translocation through the pore.

Translocation probability as a function of φ_t, σ_t

Translocation probability to the *trans*-side P_t is defined as the ratio of successful translocation events toward the *trans*-side (right) to the total number of successful translocation events that have occurred. The probability of the polymer moving to the free *cis*-side (left) is denoted by P_c and note for this study of one-sided crowding, we always set $\varphi_c = 0$, representing the free environment. Figure 7A shows the probability of the polymer to translocate to the *cis*-side (P_c) as a function of the packing fraction φ_t, for different values of σ_t. With increasing φ_t, P_c rapidly increases ($P_c = P_t = 0.5$ at $\varphi_c = \varphi_t = 0$) and eventually approaches saturation ($P_c = 1$). This indicates that, for the difference in crowding concentration on either side, the polymer prefers moving to the free *cis*-side. It can be understood on the basis of entropic ground and osmotic pressure. *Cis*-side has a more free volume, which drives the polymer to translocate to the free side to achieve a higher entropy state by minimizing the crowding-induced constrained configurations. Additionally, the concentration gradient of the crowders also plays an important role in pushing the polymer from the crowded *trans*-side to the free *cis*-side. Whereas for P_t varying with φ_t at a fixed σ_t shows complementary decrease ($P_t = 1 - P_c$) in its value (Figure 7B). This also manifests the same effect of entropy and osmotic pressure. In Figures 7C and 7D we represent how P_c and P_t varies with σ_t for different values of φ_t. We observe that P_c decreases and P_t increases monotonically with increasing σ_t for different φ_t. This trend continues for the lowest φ_t until it reaches the equal probable case $P_t \approx P_c \approx 0.5$ at maximum σ_t. While with increasing φ_t, and for lower values of σ_t, the curve rises slowly. Correspondingly for the highest φ_t, P_t starts increasing only after $\sigma_t > 3$, indicating a need for a higher σ_t to reach $P_t \neq 0$ at higher φ_t. The reason is that for a fixed φ_t on increasing σ_t, the number of crowders decreases, thereby leading to higher $\langle r_s \rangle$ between the randomly distributed crowders, resulting in the existence of large voids on the *trans* side that a polymer can explore and thereby increasing the tendency of the polymer to translocate to the crowders side. Additionally, this behavior simply corresponds to having effective osmotic pressure from the crowders on the *trans*-side. The concentration gradient created by crowders from the *trans*-side to the *cis*-side, that is, from higher osmotic pressure to the lower one, also drives the polymer to move to the free *cis*-side. For the highest packing fraction of the crowders $\varphi = 0.3$, with increasing σ_t, crowders have more large voids resulting in more free volume for the polymer to explore and also osmotic pressure at the *trans*-side is comparatively less by higher σ_t (lower ρ_c) than that by lower σ_t (higher ρ_c) and polymer prefers to stay toward the crowder side which is reflected in P_t curve. In Figure 9 we construct phase plots for P_c and P_t in the $\varphi_t - \sigma_t$ plane. P_c is maximum for higher φ_t and relatively smaller crowders (see Figure 9A, $\varphi_t > 0.1$, $\sigma_t < 1$), indicating translocation toward the free-cis side occurs more readily in a densely crowded medium with smaller crowding particles. While for the case of bigger crowders size σ_t, the effect of crowders to push the polymer to the free-cis side decreases because of the presence of larger voids in the trans side and probability of translocation to the trans side increases $P_t > 0$. Figure 9B is the complimentary phase plot of Figure 9A.

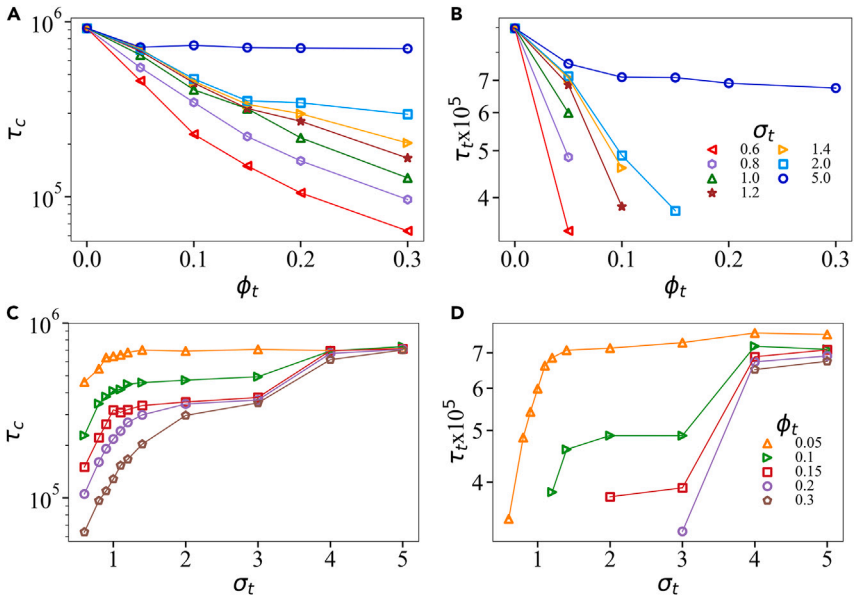

Figure 10. Translocation time as a function of φ, σ_t

Upper Panel: Translocation time as a function of packing fraction of inert crowders φ_t on the *trans*-side.

(A) Translocation time τ_c to the free *cis*-side for different σ_t.

(B) Translocation time τ_t to the crowded *trans*-side for different σ_t.

Lower Panel: Translocation time as a function of size of inert crowders σ_t on the *trans*-side.

(C) Translocation time τ_c to the free *cis*-side for different φ_t.

(D) Translocation time τ_t to the crowded *trans*-side for different φ_t.

Translocation time as a function of φ, σ_t

Now, we study the effect of packing fraction and crowder size on translocation time. Here, the system of interest consists of both polymer and crowder on the *trans*-side. Both entities owe different time scales. In 2D, for a crowder moving with a diffusion constant $D_0 = \frac{K_B T}{\xi}$, the time-scale associated with the movement to a distance of the order of their size σ is

$$\tau_0 = \frac{\sigma^2}{4D_0} = \frac{\sigma^2 \xi}{4k_B T}, \qquad \text{(Equation 11)}$$

where k_B is the Boltzamnn constant and T is absolute temperature. For the bigger crowder of diameter σ_t, time is τ

$$\tau = \frac{\sigma_t^2}{4D}. \qquad \text{(Equation 12)}$$

Therefore,

$$\tau = \tau_0 \frac{\sigma_t^2}{\sigma_0^2}. \qquad \text{(Equation 13)}$$

It shows that the timescale for diffusive motion is proportional to the damping constant and the size of the crowder. For same ξ, the τ increases rapidly on increasing σ_t.[50] As per the Rouse model, the polymer is represented as a chain having N beads. The diffusion coefficient of the Rouse chain is obtained by Einstein's relation $D_R = \frac{k_B T}{\xi_R}$. The polymer diffuses a distance of the order of its size during a characteristic time, called Rouse time τ_R is[14,50,61]

$$\tau_R = \tau_0 N^{(1+2\nu)}, \qquad \text{(Equation 14)}$$

where ν is the flory exponent. As polymers exhibit self-similarity, they are characterized by N distinct relaxation modes. Each relaxation mode is designated by a mode index $p = 1, 2, 3, \cdots, N$ can be written as

$$\tau_p = \tau_0 \left(\frac{N}{p}\right)^{(1+2\nu).} \qquad \text{(Equation 15)}$$

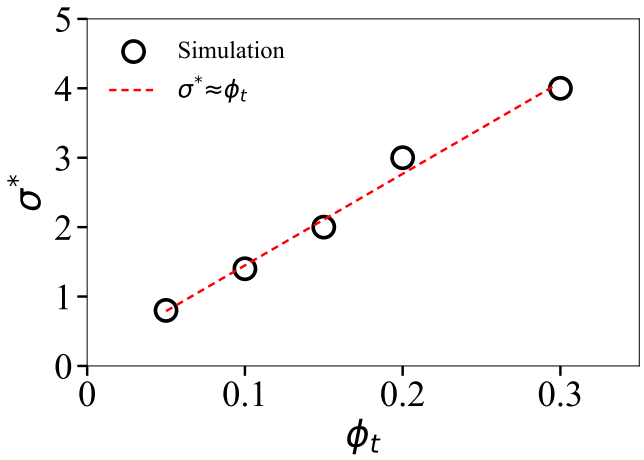

Figure 11. Sigma splitting

Packing fraction of the crowder on *trans*-side φ_t as a function of the critical value of sigma $\sigma_t \approx \sigma^*$, that is, the size of crowders above which polymer have non-zero P_t. At the critical size σ^*, the strongest effect of small crowders weakens leading to $P_t > 0$.

Within the system, the polymer is a large object that moves slowly, while the crowder movement depends on their size. In cases where the time scales for the crowder is shorter than $\tau_p = \tau_0$ for $p = N$, the correlation between the crowders is insignificant, and they provide a uniform random background for the polymer. However, when the two-time scales are comparable, as in this study, the polymer's motion correlates with the crowder's. As the size of the crowder increases, their correlations become stronger. On increasing the packing fraction of crowders, the diffusion coefficient of polymer and crowder decreases, which means correlations between the crowders become stronger. τ_t and τ_c is the time the polymer takes to translocate to the crowded trans side and to the free *cis*-side. In Figures 10A and 10B we have plotted τ_c and τ_t as a function of φ_t for different σ_t. τ_c decreases monotonically with increasing φ. A decrease in overall τ_c can be understood in terms of mean entropic force. On this basis, an increase in φ_t and random distribution of crowders on the *trans*-side will lead to lower entropy on this side and drive the polymer to translocate to the side of no crowder having higher entropy. Hence, in less time, τ_c as compared to τ_t polymer gets translocated to no crowding side. A sudden jump in the graph for higher σ_t can be interpreted from Figures 10C and 10D. It shows that translocation time is a function of σ_t for different φ_t. τ_c increases with an increase in σ_t and a decrease in φ_t. The increase in τ_t is more rapid as compared to the τ_c. For a fixed φ_t, on larger σ_t, the case of translocation to *trans*-side becomes less probable, leading to higher translocation time. Specifically, for higher σ_t, that is, $\sigma_t \geq 3$, the increase in the size of crowders on the *trans*-side leads to a rare, large void and more space for the polymer to move. Hence, the τ_t shows a sudden increase in its value. Also, in terms of osmotic pressure, as the number of crowders increases, the force exerted by them on the polymer also increases. For a fixed φ_t and the fixed area of the box on the *trans*-side, the N_t has a direct relation with the force exerted by them on the polymer and an inverse relation with the square of the size of the crowder. This also manifests the sudden jump in τ_t behavior (Figure 10D). Unlike Kaifu and Luo et al.,[50] there is no resistive force on the polymer translocation (even in the case of one side free crowders where the polymer has more entropy to go to the *cis*-side but prefers *trans*-side having bigger crowder) in fact polymer translocation to *trans*-side is effectively increased for higher σ_t.

It is expected for one-sided crowders that translocation to the free *cis*-side will always be preferred. For small crowding sizes, when the effect of the packing fraction is the strongest, there is almost 100% certainty that the polymer will translocate to the cis side, leaving $P_t = 0$. However, we have already discussed that as we increase the crowding size σ_t for the same φ, the effective impact of the crowding environment weakens and gives rise to non-zero P_t. For any specific value of φ, there is minimum σ_t, say σ^*, from where P_t starts to become $P_t > 0$. This minimum value of σ_t, we define as critical size σ^* (Figure 11). It will be interesting to observe how this critical value of crowder size σ^* depends on the packing fraction φ. Note from Figure 7C that these σ^*, the critical values of σ_t, increase with φ_t and follows an almost linear relation, $\varphi_t \approx \sigma^*$. This can be understood on the basis of entropy where the voids created on crowded *trans*-side provide a large room and hence higher entropy for the polymer to explore than from *cis*-side, which results in a non-zero P_t.

Effect of the asymmetric initial configuration of polymer on translocation probability

For the initial part of our study, we investigated the translocation dynamics of a polymer through a pore in the presence of free and one-sided crowder. Specifically, we have examined the dynamics of the polymer when it passes with its middle monomer at the pore between *cis* and *trans* side of the box. In the free case, when there are no crowders, the environment is symmetric, and a symmetrically placed polymer with a middle monomer at the pore exhibits an equal probability of translocation to either side ($P_c = P_t = 0.5$). The introduction of crowders on one side of the box breaks the symmetry in the translocation dynamics of the polymer, resulting in a preference for translocation in the direction of lower osmotic pressure and higher entropy ($P_c = 1, P_t = 0$).[47,67,70] Now, we look at how we can overcome the translocation barrier imposed by the crowders by introducing asymmetry to its length. To restore the symmetric behavior observed in the absence of crowders, we positioned the polymer asymmetrically on the side with crowders and provided it with an extra shifted length see Figures S2 and S3; Video S4. Our

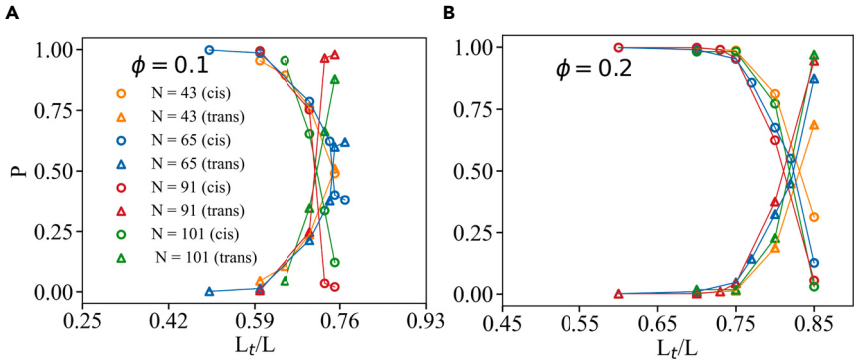

Figure 12. Effect of asymmetrically placed polymer on translocation probability

Shifting of polymer length in the crowded *trans*-side.

(A) Sparse crowding at φ_t = 0.1.

(B) Comparatively dense crowding at φ_t = 0.2 with polymer length, N = 43, 65, 91, and 101.

study suggests that the additional length of the polymer provides an edge to the crowders, allowing them to bias the direction of translocation more effectively. Figure 12 represents the translocation probability P to either side with the ratio of shifted length L_t of the polymer of length L. The first case is a polymer shifting from a sparsely crowded environment of φ = 0.1 (Figure 12A) with different lengths to a densely packed crowding φ = 0.2 (Figure 12B). As the polymer shifts to the *trans*-side where crowders reside, the likelihood of the polymer crossing over to the free *cis*-side begins to decrease from its maximum value. This decrease is due to a reduction in the length of the polymer on the *cis*-side, resulting in a decrease in available conformational entropy. A channel exists in the vicinity of the pore. The cylindrical nanochannel created by the crowders provides confinement to the polymer, resulting in a lower available area for the polymer to dangle freely. As we increase the asymmetry by shifting the polymer more to the crowder side, the confinement produced by the crowders in the pore's proximity constrains the motion on the free side due to propagation through the backbone of the polymer. Once an interesting situation arises where the polymer on the crowder side has more freedom to move compared to the confined part of the channel on the *cis* -side, which gives the polymer the push to move toward the crowder side. Howsoever, the length of the polymer, this channel will compensate for its effect on either side of the pore. This can also be interpreted in terms of entropy, the *trans* side being crowded and having more monomers due to shifted length by which configurational entropy increases; hence, the driving force for the polymer to move toward the crowders side increases. Consequently, there is an increase in the P_t value. The two curves converge at a shifted length of L_t/L, where the probability of translocation to either side is 50%, making the polymer unbiased. On shifting polymer length toward the crowders, they create a higher resistance for the polymer as it tries to translocate through the pore. As the crowding level increases for higher φ_t (Figure 12B), the polymer experiences more resistance, and the probability of translocating toward either side becomes balanced at higher shifted length. A comparative plot for both packing fractions comprising of shifted length against the total length of the polymer is shown in Figure 13. On the crowded trans side, the free energy equation remains F = E-TS but with a substantial positive E value (repulsive interactions with crowders and polymer). This results in higher free energy compared to the cis side, leading to lower entropy on the trans side. Introducing asymmetry by shifting the polymer to the trans side increases the number of monomers on the trans side, elevating the interaction energy contribution for the shifted length. Simultaneously, the shifted polymer enhances the configurational entropy on the trans side compared to the dangling tail on the cis side. The net effect is a decrease in the free energy of the chain and higher entropy on the trans side, facilitating translocation toward the crowded trans side.

Effect of both sided crowders

Now, we study the translocation dynamics of a flexible polymer driven by both side crowders to mimic environments similar to biological situations and *in vitro* setups (Figure 1C and Video S5). In this study, we kept both side packing fractions equal: $\varphi_c = \varphi_t$ and varied the relative size of the crowders. For simplicity, we always kept the *cis*-side crowding size fixed at $\sigma_c = 1$ and varied the *trans*-side crowding size σ_t (Figure 14). To start, we positioned the middle monomer $((N-1)/2)$ of the polymer chain at the pore and allowed the beads in the chain to reach equilibrium conformations through thermal collisions. Once the equilibration is completed, the polymer achieves a random configurational state, which is considered to be the initial confirmation for the translocation process. A successful translocation occurred when the polymer chain ended up on either side of the pore within the simulation time. For successful translocations, we have observed translocation probability and time as a function of packing fraction φ and crowding size σ_t. This phenomenon of polymer translocation driven by crowders can be elucidated by quantifying the average distance among the crowders $\langle r_s \rangle$ and mean entropic force $\langle F_r \rangle$. Consider that there are N_c crowders in general of the diameter σ_i on either side of the box with dimension ($L_x \times L_y$), then the packing fraction is

$$\varphi = \frac{N_c \pi \left(\frac{\sigma_i}{2}\right)^2}{L_x \times L_y}. \quad \text{(Equation 16)}$$

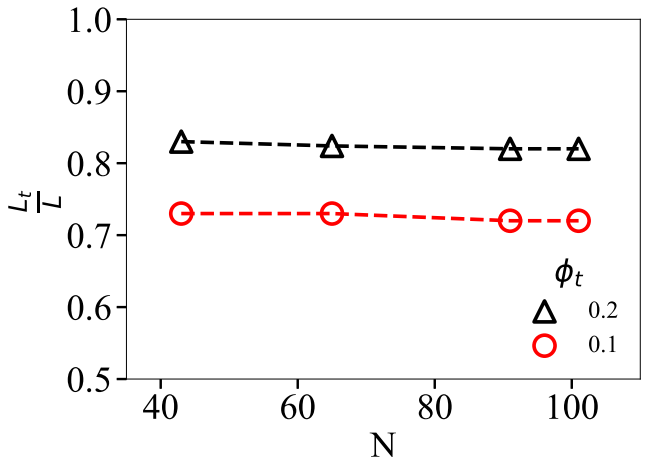

Figure 13. Polymer length shifted (L_t/L) toward crowded environments for equal translocation probability

Plot of the fraction of the shifted length of the polymer (L_t/L) with respect to symmetric configuration *vs* the length of the polymer *N* for two different packing fraction $\varphi_t = 0.1, 0.2$. The fraction of the length need to be shifted towards the crowding side to get back an equal *cis* and *trans* translocation probability is independent of the length of the polymer.

Using Equation 17 and alike Equation 7, the average distance between the surface of the crowders $\langle r_s \rangle$ is

$$\langle r_s \rangle = \sigma_i \left(\frac{1}{2} \sqrt{\pi/\varphi} - 1 \right), \quad \text{(Equation 17)}$$

The packing fraction of crowders at both sides is set as $\varphi_t = \varphi_c = \varphi$, and the size of the crowder at the *cis*-side is kept fixed $\sigma_i = \sigma_c = 1$. On the trans side, the size of the crowder varies $\sigma_t = \sigma_i$ within $0.6 \leq \sigma_t \leq 2.5$ for our case. Thus, the average distance between the surface of the *cis*-side crowders $\langle r_{cs} \rangle$ and *trans*-side crowder $\langle r_{ts} \rangle$ is

$$\langle r_{cs} \rangle = \sigma_c \left(\frac{1}{2} \sqrt{\pi/\varphi} - 1 \right), \langle r_{ts} \rangle = \sigma_t \left(\frac{1}{2} \sqrt{\pi/\varphi} - 1 \right). \quad \text{(Equation 18)}$$

Equations 17 and 18 indicates that for a fixed φ, $\langle r_s \rangle$ increase with increasing σ_i and it decreases with increasing φ for a fixed σ_i. It will provide insight into understanding the phenomena of translocation induced by crowders and the average distance between their surfaces. As the polymer is coming out of a pore, crowders create a confined cylindrical channel of size $\langle r_s \rangle$. For this mean entropic force $\langle F_r \rangle$ can be written as[50,66,67]

$$\langle F_r \rangle = F_0 \frac{k_B T}{\langle r_s \rangle}, \quad \text{(Equation 19)}$$

where F_0 is the proportionality constant, k_B is the Boltzmann constant, T is the absolute temperature. Simplifying the expression of $\langle F_r \rangle$ for cis and *trans*-side crowder in terms of $\langle r_{cs} \rangle, \langle r_{ts} \rangle$, σ_c, σ_t, and φ gives

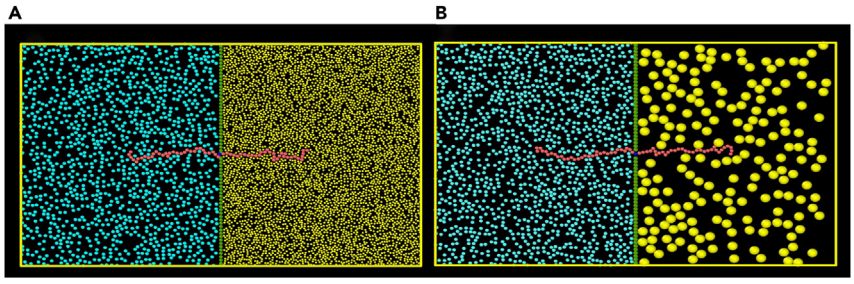

Figure 14. Translocation dynamics in the both-sided crowded environment

Schematic illustration of polymer translocation process through a pore with asymmetric crowders on both sides of the box. The size of crowders on the *cis*-side is kept fixed $\sigma_c = 1$. The size of crowders on *trans*-side σ_t keeps on changing while keeping the packing fraction on both sides alike ($\varphi_t = \varphi_c = \varphi$).

(A) Packing fraction of crowders on both sides $\varphi = 0.3$ (densely crowded) while $\sigma_c = 1$ and $\sigma_t = 0.6$ (case: $\sigma_t < \sigma_c$).

(B) Packing fraction of crowders on both sides $\varphi = 0.3$ while $\sigma_c = 1$ and $\sigma_t = 4$ (case: $\sigma_t > \sigma_c$).

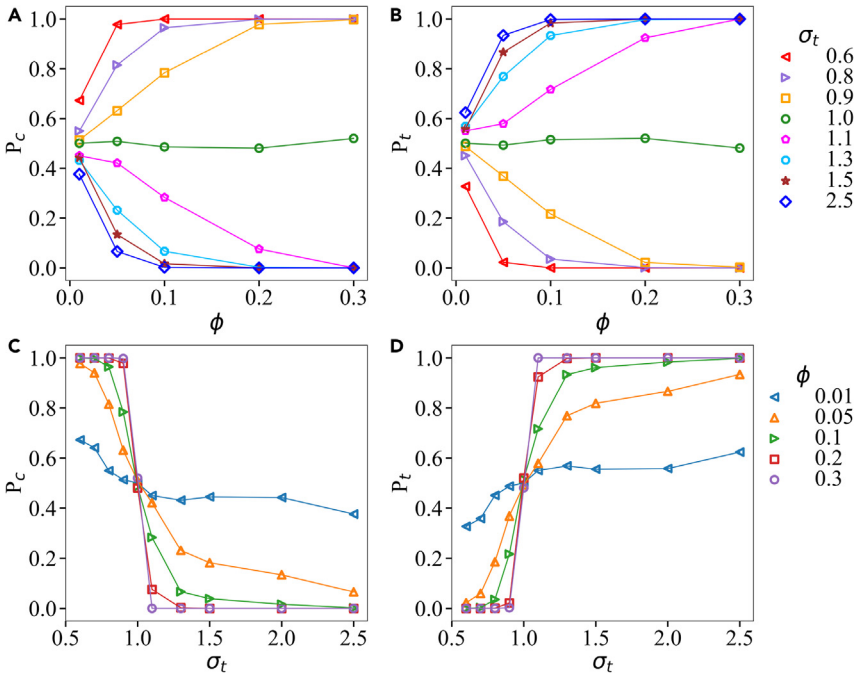

Figure 15. Translocation probability as a function of φ, and σ_t

Upper panel: Translocation probability as a function of packing fraction φ.

(A) Translocation probability P_c to *cis*-side vs φ for different σ_t.

(B) Translocation probability P_t to *trans*-side vs φ for different σ_t. Lower panel: Translocation probability as a function of σ_t of inert crowders on the trans side.

(C) Translocation probability P_c to *cis*-side vs σ_t for different φ_t.

(D) Translocation probability P_t to *trans*-side vs σ_t for different φ_t.

$$\langle F_r \rangle = F_0 k_B T \left(\frac{1}{\langle r_{cs} \rangle} - \frac{1}{\langle r_{ts} \rangle} \right), \quad \text{(Equation 20)}$$

$$\langle F_r \rangle = F_0 k_B T \frac{1}{\frac{1}{2}\sqrt{\pi/\varphi} - 1} \left(\frac{1}{\sigma_c} - \frac{1}{\sigma_t} \right). \quad \text{(Equation 21)}$$

Equation 21 show that $\langle F_r \rangle$ depends on φ and varying *trans*-side crowders of σ_t. With increasing φ or changing σ_t keeping σ_c fixed, $\langle F_r \rangle$ increases.[50] Polymer prefers to move the size of bigger crowders due to larger conformational entropy. Further, Osmotic pressure (Π), which is a colligative property, depends on the number density of the crowder and influences the translocation dynamics. We put a polymer chain at the center of the wall, separated by a difference in crowding size, which creates a crowding concentration gradient on either side. The polymer chain will be driven by the difference in osmotic pressure created by the concentration gradient and prefers to stay on the side of relatively lower osmotic pressure and higher volume. Thus, the competition between mean entropic force and osmotic pressure determines the direction of the translocation process.

Translocation probability as a function of φ, and σ_t

The probability of polymer translocating to the *cis*-side and *trans*-side is represented by P_c and P_t, respectively. In Figures 15A and 15B, we have plotted the translocation probability of the polymer as a function of the packing fraction φ for different σ_t, note σ_c is always kept constant at $\sigma_c = 1$. Plot shows bifurcation from equally probable scenario ($P_t = P_c = 0.5$ at $\sigma_t = 1$) to two opposite extremes ($\sigma_t \neq \sigma_c$). For $\sigma_t \leq \sigma_c$, the polymer has a tendency to move to the cis side where bigger crowder resides. P_c rapidly increases from 50 to 50 % at lower φ and then slowly reaches its maximum value at higher φ. While for the case of $\sigma_t \geq \sigma_c$, the polymer has a tendency to move to the trans side. This indicates that for the same φ on both sides, translocation is preferred to the side of bigger crowders. This behavior is reminiscent of the effect of osmotic pressure, which provides a push to the polymer to translocate from a higher crowder concentration to a lower concentration side. For the same φ, osmotic pressure (Π) at the side of the smaller crowder is higher than that of the side of a bigger one, leading to the polymer moving to the bigger crowder side. Such behavior of probability with φ for polymer translocation through pore have been reported earlier.[50] We next look at the translocation probability of the polymer as a function of σ_t for different φ. P_t displays distinct features as σ_t is varied (Figures 15C and 15D). For $\sigma_t < \sigma_c$ till it reaches $\sigma_t = 1$, that is, for the relatively small *trans*-side crowders, polymer translocates to the *cis*-side ($P_t = 0$). But,

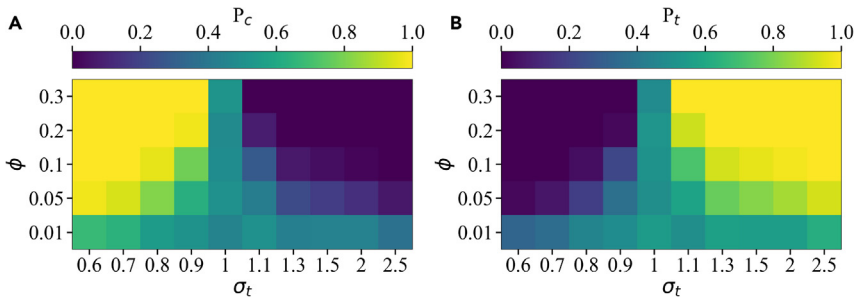

Figure 16. Phase plot of translocation probability in $\varphi - \sigma_t$ plane

The plot elucidates how translocation probabilities P_c and P_t vary as the function of the size of crowders on the trans side (σ_t) and their packing fraction (φ) in a both-sided crowded environment. The size of crowders on the cis side is kept fixed at $\sigma_c = 1$, and the packing fraction of both sides is kept equal, that is, $\varphi_c = \varphi_t = \varphi$. It shows a switch in the direction of translocation of a polymer by tuning crowding size.

(A and B) Translocation probability to *cis*-side and *trans*-side respectively.

the moment there is a crossover of $\sigma_t = 1$, the curve shows a sudden jump in its behavior from its lowest to saturation ($P_t = 1$). This sudden switch prevails over the higher σ_t for the highest $\varphi = 0.3$ and shows a fall from $P_t = 1$ for decreasing φ. Additionally, even for $\varphi = 0.01$, which is almost a crowder-free environment, the strong effect of tiny crowders ($\sigma_t < \sigma_c$) pushes the polymer to translocate to the *cis*-side ($P_t = 0.3$). While for the same $\varphi = 0.01$ at $\sigma_t > \sigma_c$, the polymer has an equal probability of moving to either side as it is like a tug-of-war situation. This result can be interpreted in terms of the mean radial entropic force. $\langle F_r \rangle$ increases with increasing σ_t and φ and hence leads the translocation dynamics. Unlike Chen et al., 2013,[50] our model has no bottleneck or resistive force pertaining to non-monotonic behavior. The results in Figure 15 are relevant to the simulation study by Chen and Luo.[50] They observed that the polymer with an initial configuration where the middle monomer at the pore on the wall separating two sides will prefer to translocate to the side of bigger crowders. They note that polymer that goes to the side of a bigger crowder exhibits a maximum probability on increasing σ up to a certain extent and then shows a downfall due to the interplay of the driving force and the resistive force, specifically from the bottleneck leading to the non-monotonic behavior of probability. They observed that at large σ, it shows the resistive force of large magnitude compensated by entropic force leads to a decrease in probability to the bigger crowder side. While, in our case, the calculations are consistent with Chen and Luo and likewise to Polson,[57] our model also contradicts this and denies any bottleneck in the system pertaining to non-monotonicity in the curve. In our case, the probability curve exhibits a continuous increase as the polymer prefers to translocate to the side of bigger crowders and does not account for the downfall in the curve is noted. The behavior of the crossover region of $\sigma_t = 1$ as a function of φ is presented in phase plot for P_c and P_t in $\varphi - \sigma_t$ plane (Figure 16). P_c is maximum for smaller σ_t and higher φ_t (see Figure 16A, $\sigma_t < 1, \varphi > 0.05$). For relatively bigger crowders, the phase plot shows a uniform increase in P_t with increasing σ_t for all φ (see Figure 16B).

Translocation time as a function of φ, and σ_t

We first look at the translocation time as a function of packing fraction φ for different values of crowder size σ_t (Figures 17A and 17B). Owing to an alike environment on both sides of the pore for $\sigma_t = \sigma_c = 1$, the overall τ owes the highest value. Further diverging from $\sigma_c = \sigma_t = 1$ and moving to the asymmetric nature of crowded size ($\sigma_c \neq \sigma_t$), we observe a decrease τ_c and τ_t with increasing φ for both the situation: $\sigma_t < \sigma_c$, and $\sigma_t > \sigma_c$. This result can be elucidated in the context of $\langle F_r \rangle$, which increases on increasing φ. For $\sigma_t < \sigma_c$, the combined effect of osmotic pressure Π and mean entropic force $\langle F_r \rangle$ moves the polymer to lower crowding concentration and higher entropy which dominate the translocation phenomenology and drives the polymer on bigger crowder side of the pore ensuing lower τ_c (Figure 17A) and for $\sigma_t > \sigma_c$ holds the higher value of the average distance between the surface of crowder on *trans*-side than on the cis side, providing more space for the polymer to translocate easily in lesser time τ_t (Figure 17B). Additionally, translocation is a stochastic process, and random fluctuations could lead the polymer to move to either the cis or trans side. But it's not necessary that translocation would occur for all particular cases, and pointed out translocation at these points is a very rare event since we introduced biases in the form of crowders in extreme bias, we wouldn't observe any translocation event taking place to the unfavored side. In Figure 17A, translocation time values corresponding to $\sigma_t = 0.8, 2.0$ are not present at certain values of φ. This absence is attributed to the rare and stochastic nature of translocation events. The lack of translocation time values on either side indicates the non-occurrence of translocation in that specific direction. To elaborate, when translocation doesn't occur on the cis side at a given time, but the polymer successfully translocates to the trans side, the corresponding translocation time values are reflected in Figure 17B. We next look at the situation for translocation time varying with σ_t for different φ (Figures 17C and 17D). At lower $\sigma_t < \sigma_c$, τ_c rises faster for higher φ. On the other hand for $\sigma_t > \sigma_c$, τ_t shows decreasing behavior on increasing φ. As explained earlier, the combined effect of Π, $\langle F_r \rangle$, $\langle r_s \rangle$ pulls the polymer rapidly to the side of bigger crowder (Figures 17C and 17D).

Effect of crowding size on translocation probability

Translocation for the case of no crowders provides us the 50 − 50% probability ($P_c \approx P_t \approx 0.5$). Initially, the symmetry of the environment of obtaining equal probable case has been broken by introducing crowders on one side ($P_c = 1, P_t = 0$). We have observed that most of the

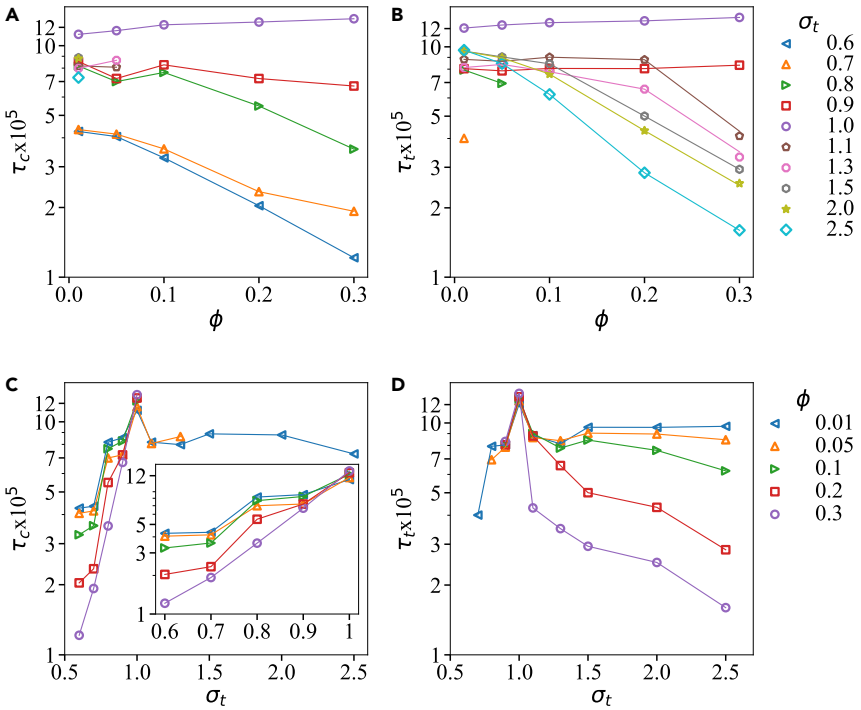

Figure 17. Translocation time as a function of φ, and σ_t

Upper Panel: Translocation time as a function of packing fraction φ_t.

(A) Translocation time τ_c to the *cis*-side vs φ for different σ_t.

(B) Translocation time τ_t to the *trans*-side vs φ for different σ_t. Lower Panel: Translocation time as a function of size of inert crowders σ_t on the *trans*-side.

(C) Translocation time τ_c to the *cis*-side vs σ_t for different φ_t.

(D) Translocation time τ_t to the *trans*-side vs σ_t for different φ_t.

time polymer is translocating to the side of the crowders on the grounds of mean entropic force, osmotic pressure, and distance between the surface of the crowders. Next, the symmetry has been broken by introducing asymmetry in the initial configuration of the polymer, that is, shifting the length toward the crowder side. A ratio of L_t/L exists where the equal probable case of cis and *trans*-translocation is retrieved. Now, when the crowders are being introduced on both sides of the box, we have investigated that the polymer is translocating almost to the side of bigger crowders ($P_c = 0, P_t = 1$ for $\sigma_t < \sigma_c$, and $P_c = 1, P_t = 0$ for $\sigma_t > \sigma_c$). Similarly, in this case, to restore an equal probability scenario, symmetry is broken by changing the packing fraction of crowders on the trans side, i.e., φ_c is not equal to φ_t anymore. We are choosing a particular value of the σ_t and varying the number of crowders N_t, which in turn changes the packing fraction φ_t. The goal is to obtain an optimum value of the packing fraction of crowders on the *trans*-side so that the polymer translocates equally to both sides rather than having a preference for the side of the bigger crowder. Figures 18A and 18B illustrate the relationship between the probability of translocation P and the ratio of packing fractions of two sides φ_t/φ_c. In Figure 18A, the crowders on the *trans*-side are larger ($\sigma_c = 4$) than those on the *cis*-side ($\sigma_c = 3$), while in Figure 18B, the *trans*-side has smaller crowders ($\sigma_c = 2$) than the *cis*-side ($\sigma_c = 3$). Both figures examine sparse and densely crowded environments of packing fraction on the *cis*-side ($\varphi_c = 0.1, 0.2$), with ($\sigma_c = 3$) held constant while N_c is fixed. N_t varies until the polymer becomes unbiased of size, packing fraction, and the number of crowders, allowing it to translocate to either side with equal probability.

DISCUSSION

Medium-driven controlled polymer translocations without any explicit external forces are fundamental problems in science and engineering. Using Langevin dynamics simulations, we extensively study the effect of crowding and polymer length distribution on the translocation processes in crowd-free and crowded environments. We investigated the scaling properties of translocation probability P, time τ, and MSD. First, we compared the scaling properties with the results generated by the standard scaling theories of polymer physics. We obtained scaling for translocation time $\tau \sim N^{2.5}$ and when $\tau > \tau_R$ MSD shows $\langle \Delta r^2(t) \rangle \sim t^{0.8}$, in free environment. Our results exactly match the experimental data and show subdiffusive behavior. A simple analysis of the average crossing time $\langle \tau_{crossing} \rangle$ of individual monomer, as it crosses the pore, has been performed and laid the foundation of two interesting but counterintuitive features of translocation rate k_T and bead velocity v_b. It has been observed that the translocation rate is minimum when the middle monomer passes the pore and keeps on increasing, whereas it holds the opposite behavior for bead velocity, which is maximum for the middle monomer and decreases for the subsequent part of tail monomers. Further, we rationalize the translocation phenomena in the light of nucleation processes. An asymmetrically placed polymer at the pore

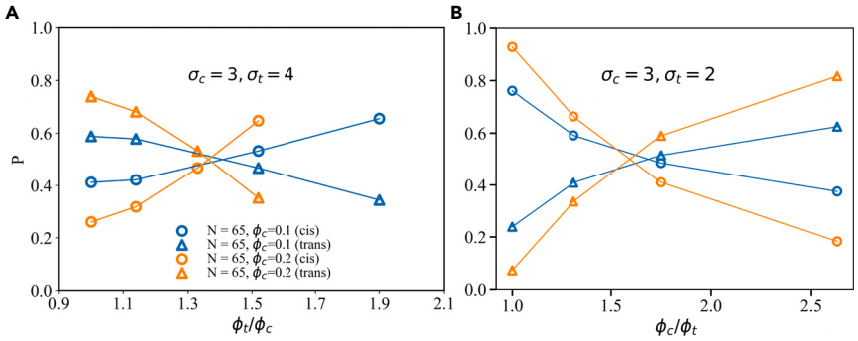

Figure 18. Effect of crowding size on translocation probability

(A)Translocation probability *P* as a function ratio of packing fraction of crowders on the *trans*-side and cis side φ_t/φ_c for two distinct values of φ = 0.1,0.2. The size of crowder on the cis side σ_c = 3 while that on the trans side σ_t = 4.

(B) The size of crowder on the cis side σ_c = 3 while that on the trans side σ_t = 2.

toward the receiver side once crosses a significant number of monomers across the pore; that is, when the nucleation barrier has been overcome and free energy maxima is reached, the probability of the polymer going back to the donor side is almost negligible. For one-sided crowding, with crowding on the trans side and free on the cis side, the translocation probability and time have been noted. P_t shows a monotonic decrease with increasing φ but shows an increase when the crowder's size σ_t is large enough to create rare, large voids the polymer can explore. This provides us with a critical value of σ_t called σ^* where the polymer has non-zero P_t and translocates to the crowded side. A complimentary behavior is also followed by P_c. A breakthrough in the existing model has been achieved by simply shifting polymer length from the middle monomer to the crowded side to examine whether there can be a situation if a crowd-free environment probability can be retraced. The study has been done for both sparse environment φ_t = 0.1 and relatively dense φ_t = 0.2 and we investigated that there exists a ratio of length shift to the polymer length L_t/L where polymer exhibits $P_t \approx P_c \approx 0.5$. Translocation time τ_t decreases rapidly with increasing σ_t and an increase with larger σ_t. In the case of two-sided crowding, where the packing fraction of both sides is set fixed, we kept the crowding side on the cis side σ_c fixed, and on the trans side, σ_t is varying. The translocation probability shows a bifurcation from the equal probable case, and polymer translocates to the side of bigger crowders, $P_t > 0.5$ for $\sigma_t > \sigma_c$ and $P_t < 0.5$ for $\sigma_t < \sigma_c$. The probability curve shows a sudden switch from its lowest to peak value when a crossover of $\sigma_t = \sigma_c$ happens. Translocation time τ_t decreases with increasing φ and σ_t, indicating the polymer preference to stay toward bigger crowders in less time. A study on changing the relative packing fraction of crowders on both sides leads to the 50 − 50 probability akin to the crowd-free situation is done. These results can be interpreted by the interplay between mean entropic force and effective osmotic pressure of the crowders. In the case of driven translocation, when an external force is applied on the polymer up to its certain length and after that, if the force is switched off, then the entropy-driven force and free energy are sufficient to keep the polymer on the preferred side. Our model is generally enough to switch the translocation direction without any explicit force. Once the nucleation barrier is crossed for successful translocation, the polymer has an almost extremely low probability of going back to the donor side. In other words, the regulation of the free energy barrier by tuning the polymer length can have significance in the translocation phenomena having biomedical applications, for example, in the field of controlled drug delivery systems. Further, both spatial and temporal control over the translocation of a polymer tethered to a surface can be incorporated into our model. In the context of targeted drug delivery systems, we aim to deliver drugs specifically to designated cells, organelles, etc. This is the direct and potential application of polymer translocation, allowing us to control the direction of polymer translocation in accordance with the target's environment.[71–73] Controlled translocation of single molecules can be achieved by maintaining control over the nanopore in such a way that we have a speed tuning of individual beads and molecules as well as passing through it at the desired time; that is, molecule-independent speed control can be achieved.[30]

STAR★METHODS

Detailed methods are provided in the online version of this paper and include the following:

- KEY RESOURCES TABLE
- RESOURCES AVAILABILITY
  - Lead contact
  - Materials availability
  - Data and code availability
- METHOD DETAILS
- QUANTIFICATION AND STATISTICAL ANALYSIS

SUPPLEMENTAL INFORMATION

Supplemental information can be found online at https://doi.org/10.1016/j.isci.2024.109348.

ACKNOWLEDGMENTS

We would like to thank Jaeoh Shin, Praveen Bommineni, Kunal Rai, and Thyageshwar Chandran for their useful discussion and critical comments. VG and SKG would like to thank SERB, DST (Project No. SRG/2020/001606) for funding. SKG would like to thank SERB, DST (Project No. MTR/2022/000833) for financial support. We want to acknowledge NIT Warangal for the research seed funds and institute fellowship to VG.

AUTHOR CONTRIBUTIONS

Conceptualization, V.G., R. M., K.S., and S.K.G.; Methodology, V.G., R.M., R.I., and S.K.G.; Software: V.G. and R.M.; Validation: K.S. and S.K.G.; Formal Analysis: V.G., R.M., and S.K.G.; Investigation, V.G., R.M., and S.K.G.; Writing – Original Draft, V.G.; Writing – Review and Editing, V.G., R.M., R.I., K.S., and S.K.G.; Data Curation: V.G. and R.M.; Visualization: V.G. and R.M.; Project Administration: S.K.G.; Funding Acquisition, S.K.G.; Resources, S.K.G.; Supervision, S.K.G.

DECLARATION OF INTERESTS

The authors declare no competing interests.

Received: November 3, 2023
Revised: January 29, 2024
Accepted: February 23, 2024
Published: February 28, 2024

REFERENCES

1. Butler, T.Z., Gundlach, J.H., and Troll, M.A. (2006). Determination of RNA orientation during translocation through a biological nanopore. Biophys. J. *90*, 190–199.
2. Dubbeldam, J.L.A., Milchev, A., Rostiashvili, V.G., and Vilgis, T.A. (2007). Polymer translocation through a nanopore: A showcase of anomalous diffusion. Phys. Rev. *76*, 010801.
3. Meller, A., Nivon, L., Brandin, E., Golovchenko, J., and Branton, D. (2000). Rapid nanopore discrimination between single polynucleotidemolecules. Proc. Natl. Acad. Sci. USA *97*, 1079–1084.
4. Howorka, S., Cheley, S., and Bayley, H. (2001). Sequence-specific detection of individual DNA strands using engineered nanopores. Nat. Biotechnol. *19*, 636–639.
5. Vercoutere, W., Winters-Hilt, S., Olsen, H., Deamer, D., Haussler, D., and Akeson, M. (2001). Rapid discrimination among individual DNA hairpin molecules at single-nucleotide resolution using an ion channel. Nat. Biotechnol. *19*, 248–252.
6. Singh, K., Ghosh, S.K., Kumar, S., and Sain, A. (2013). Stretching-force–dependent transitions in single stranded DNA. Europhys. Lett. *100*, 68004. https://doi.org/10.1209/0295-5075/100/68004.
7. Nakane, J., Wiggin, M., and Marziali, A. (2004). A nanosensor for transmembrane capture and identification of single nucleic acid molecules. Biophys. J. *87*, 615–621.
8. Muthukumar, M. (2001). Translocation of a confined polymer through a hole. Phys. Rev. Lett. *86*, 3188–3191.
9. Zhou, Y., and Wang, H. (2022). Molecular Dynamics Simulation of a Single Carbon Chain through an Asymmetric Double-Layer Graphene Nanopore for Prolonging the Translocation Time. ACS Omega *7*, 16422–16429.
10. Citovsky, V., and Zambryski, P. (1993). Transport of nucleic acids through membrane channels: snaking through small holes. Annu. Rev. Microbiol. *47*, 167–197.
11. Singh, K., and Sain, A. (2013). How helix-coil transition influences translocation of a singlestranded DNA and kinetics of its fluctuation inside the channel. Europhys. Lett. *104*, 18007. https://doi.org/10.1209/0295-5075/104/18007.
12. Theeyancheri, L., Chaki, S., Bhattacharjee, T., and Chakrabarti, R. (2022). Migration of active rings in porous media. Phys. Rev. E *106*, 014504.
13. Di Marzio, E.A., and Mandell, A.J. (1997). Phase transition behavior of a linear macromolecule threading a membrane. J. Chem. Phys. *107*, 5510–5514.
14. Doi, M., Edwards, S.F., and Edwards, S.F. (1988). The Theory of Polymer Dynamics*73* (oxford university press).
15. Sung, W., and Park, P. (1996). Polymer translocation through a pore in a membrane. Phys. Rev. Lett. *77*, 783–786.
16. Kasianowicz, J.J., Henrickson, S.E., Misakian, M., Weetall, H.H., Robertson, B., and Stanford, V. (2002). Physics of DNA threading through a nanometer pore and applications to simultaneousmultianalyte sensing. Structure and dynamics of confined polymers, 141–164.
17. Peskin, C.S., Odell, G.M., and Oster, G.F. (1993). Cellular motions and thermal fluctuations: the Brownian ratchet. Biophys. J. *65*, 316–324.
18. Kasianowicz, J.J., Brandin, E., Branton, D., and Deamer, D.W. (1996). Characterization of individual polynucleotide molecules using a membrane channel. Proc. Natl. Acad. Sci. USA *93*, 13770–13773.
19. Pavan, K., Madasu Arpita Maity, S.K.G., and Chandran, T. (2023). Insights into the microevolution of SARS-ACE2 interactions: in silico analysis of glycosylation and SNP pattern. J. Biomol. Struct. Dyn. *41*, 6442–6449. https://doi.org/10.1080/07391102.2022.2106517.
20. Liechty, W.B., Kryscio, D.R., Slaughter, B.V., and Peppas, N.A. (2010). Polymers for drug delivery systems. Annu. Rev. Chem. Biomol. Eng. *1*, 149–173.
21. Bettini, R., Catellani, P.L., Santi, P., Massimo, G., Peppas, N.A., and Colombo, P. (2001). Translocation of drug particles in HPMC matrix gel layer: effect of drug solubility and influence on release rate. J. Contr. Release *70*, 383–391.
22. Roy, S.M., Garg, V., Sivaraman, S.P., Barman, S., Ghosh, C., Bag, P., Mohanasundaram, P., Maji, P.S., Basu, A., Dirisala, A., et al. (2023). Overcoming the barriers of nuclear-targeted drug delivery using nanomedicine-based strategies for enhanced anticancer therapy. J. Drug Deliv. Sci. Technol. *83*, 104408. https://doi.org/10.1016/j.jddst.2023.104408.
23. Ge, H., and Wu, C. (2010). Separation of Linear and Star Chains by a Nanopore. Macromolecules *43*, 8711–8713.
24. Ali, I., and Yeomans, J.M. (2005). Polymer translocation: The effect of backflow. J. Chem. Phys. *123*, 234903.
25. Lubensky, D.K., and Nelson, D.R. (1999a). Driven polymer translocation through a narrow pore. Biophys. J. *77*, 1824–1838.
26. Sarabadani, J., Metzler, R., and Ala-Nissila, T. (2022). Driven polymer translocation into a channel: Isoflux tension propagation theory and Langevin dynamics simulations. Phys. Rev. Res. *4*, 033003.
27. Hsiao, P.-Y. (2020). Translocation of a Polyelectrolyte through a Nanopore in the Presence of Trivalent Counterions: A Comparison with the Cases in Monovalent and Divalent Salt Solutions. ACS Omega *5*, 19805–19819.
28. Buyukdagli, S., Sarabadani, J., and Ala-Nissila, T. (2019). Theoreticalmodeling of polymer translocation: From the electrohydrodynamics of short polymers to the fluctuating long polymers. Polymers *11*, 118.
29. Lathrop, D.K., Ervin, E.N., Barrall, G.A., Keehan, M.G., Kawano, R., Krupka, M.A., White, H.S., and Hibbs, A.H. (2010). Monitoring the escape of DNA from a nanopore using an alternating current signal. J. Am. Chem. Soc. *132*, 1878–1885.
30. Leitao, S.M., Navikas, V., Miljkovic, H., Drake, B., Marion, S., Pistoletti Blanchet, G., Chen, K., Mayer, S.F., Keyser, U.F., Kuhn, A., et al. (2023). Spatially multiplexed single-molecule translocations through a nanopore at

controlled speeds. Nat. Nanotechnol. *18*, 1078–1084.
31. Sahoo, R., and Chakrabarti, R. (2023). Structure and dynamics of an active polymer chain inside a nanochannel grafted with polymers. Soft Matter *19*, 5978–5988.
32. Kantor, Y., and Kardar, M. (2004). Anomalous dynamics of forced translocation. Phys. Rev. *69*, 021806.
33. Ollila, S.T.T., Luo, K.F., Ala-Nissila, T., and Ying, S.-C. (2009). Polymer translocation in a double-force arrangement. Eur. Phys. J. E Soft Matter *28*, 385–393.
34. Panja, D., and Barkema, G.T. (2008). Passage times for polymer translocation pulled through a narrow pore. Biophys. J. *94*, 1630–1637.
35. Ambjörnsson, T., and Metzler, R. (2004). Chaperone-assisted translocation. Phys. Biol. *1*, 77–88.
36. Luo, K., Ala-Nissila, T., and Ying, S.-C. (2006). Polymer translocation through a nanopore: A two-dimensional Monte Carlo study. J. Chem. Phys. *124*, 034714.
37. Yu, W.-C. (2020). Translocation of heterogeneous flexible polymers assisted by binding particles. Chin. J. Polym. Sci. *38*, 784–790.
38. Yu, W., and Luo, K. (2011). Chaperone-assisted translocation of a polymer through a nanopore. J. Am. Chem. Soc. *133*, 13565–13570.
39. Lubensky, D.K., and Nelson, D.R. (1999b). Driven Polymer Translocation Through a Narrow Pore. Biophys. J. *77*, 1824–1838. https://doi.org/10.1016/S0006-3495(99)77027-X.
40. Lehtola, V.V., Linna, R.P., and Kaski, K. (2010). Unforced polymer translocation compared to the forced case. Phys. Rev. *81*, 031803.
41. Simon, S.M., Peskin, C.S., and Oster, G.F. (1992). What drives the translocation of proteins? *89*, 3770–3774. https://doi.org/10.1073/pnas.89.9.3770.
42. Ghosh, S.K., Singh, K., and Sain, A. (2009). Effect of intrinsic curvature on semiflexible polymers. Phys. Rev. E *80*, 051904. https://doi.org/10.1103/PhysRevE.80.051904.
43. Luo, K., and Metzler, R. (2010a). Polymer translocation into laterally unbounded confined environments. J. Chem. Phys. *133*, 075101.
44. Wong, C.T.A., and Muthukumar, M. (2008). Scaling theory of polymer translocation into confined regions. Biophys. J. *95*, 3619–3627.
45. Lucas, F.L.R., Willems, K., Tadema, M.J., Tych, K.M., Maglia, G., and Wloka, C. (2022). Unbiased Data Analysis for the Parameterization of Fast Translocation Events through Nanopores. ACS Omega *7*, 26040–26046.
46. Luo, K., Ollila, S.T.T., Huopaniemi, I., Ala-Nissila, T., Pomorski, P., Karttunen, M., Ying, S.-C., and Bhattacharya, A. (2008). Dynamical scaling exponents for polymer translocation through a nanopore. Phys. Rev. *78*, 050901.
47. Gopinathan, A., and Kim, Y.W. (2007). Polymer translocation in crowded environments. Phys. Rev. Lett. *99*, 228106.
48. Wen, C., and Zhang, S.-L. (2021). On current blockade upon analyte translocation in nanopores. J. Appl. Phys. *129*, 064702.
49. Kramers, H.A. (1940). Brownian motion in a field of force and the diffusion model of chemical reactions. Physica *7*, 284–304.
50. Chen, Y., and Luo, K. (2013). Dynamics of polymer translocation through a nanopore induced by different sizes of crowding agents. J. Chem. Phys. *138*, 204903.
51. Luo, K., and Metzler, R. (2010b). Polymer translocation into a fluidic channel through a nanopore. Phys. Rev. *82*, 021922.
52. Meller, A., and Branton, D. (2002). Singlemoleculemeasurements of DNA transport through a nanopore. Electrophoresis *23*, 2583–2591.
53. Molcrette, B., Chazot-Franguiadakis, L., Liénard, F., Balassy, Z., Freton, C., Grangeasse, C., and Montel, F. (2022). Experimental study of a nanoscale translocation ratchet. Proc. Natl. Acad. Sci. USA *119*, e2202527119.
54. Chuang, J., Kantor, Y., and Kardar, M. (2002). Anomalous dynamics of translocation. Phys. Rev. *65*, 011802.
55. Afrasiabian, N., and Denniston, C. (2020). The journey of a single polymer chain to a nanopore. Soft Matter *16*, 9101–9112.
56. Chaudhury, S., and Cherayil, B.J. (2008). A model of anomalous chain translocation dynamics. J. Phys. Chem. B *112*, 15973–15979.
57. Polson, J.M., and Heckbert, D.R. (2019). Polymer translocation into cavities: Effects of confinement geometry, crowding, and bending rigidity on the free energy. Phys. Rev. E *100*, 012504.
58. Luo, K., Metzler, R., Ala-Nissila, T., and Ying, S.-C. (2009). Polymer translocation out of confined environments. Phys. Rev. *80*, 021907.
59. Muthukumar, M. (2016). Polymer Translocation (CRC press).
60. Shin, J., Cherstvy, A.G., and Metzler, R. (2015). Polymer looping is controlled by macromolecular crowding, spatial confinement, and chain stiffness. ACS Macro Lett. *4*, 202–206.
61. Rubinstein, M., Colby, R.H., et al. (2003). Polymer Physics*23* (Oxford university press).
62. Rezaie-Dereshgi, A., Khalilian, H., and Sarabadani, J. (2022). Translocation of an Active Polymer into a Circular Cavity. Preprint at arXiv. https://doi.org/10.48550/arXiv.2211.07115.
63. Muthukumar, M. (1999). Polymer translocation through a hole. J. Chem. Phys. *111*, 10371–10374.
64. Stauffer, D., and Aharony, A. (2018). Introduction to Percolation Theory (CRC press).
65. Essam, J.W. (1980). Percolation theory. Rep. Prog. Phys. *43*, 833–912.
66. Muthukumar, M., and Baumgärtner, A. (1989). Effects of entropic barriers on polymer dynamics. Macromolecules *22*, 1937–1941.
67. Roos, N. (2014). Entropic forces in Brownianmotion. Am. J. Phys. *82*, 1161–1166.
68. Sheng, J., and Luo, K. (2012). Ejection dynamics of a ring polymer out of a nanochannel. Soft Matter *8*, 367–374.
69. De Gennes, P.-G., and Gennes, P.-G. (1979). Scaling Concepts in Polymer Physics (Cornell university press).
70. Bhattacharjee, S.M., Giacometti, A., and Maritan, A. (2013). Flory theory for polymers. J. Phys. Condens. Matter *25*, 503101.
71. Bai, X., Li, M., and Hu, G. (2020). Nanoparticle translocation across the lung surfactant film regulated by grafting polymers. Nanoscale *12*, 3931–3940.
72. Zhang, M., Ellis, E.A., Cisneros-Zevallos, L., and Akbulut, M. (2012). Uptake and translocation of polymeric nanoparticulate drug delivery systems into ryegrass. RSC Adv. *2*, 9679–9686.
73. Maitra Roy, S., Barman, S., Kishore, P., Chatterjee, B., Bag, P., Ghatak, T., Basu, A., Ghosh, S.K., Dirisala, A., Sarkar, A.K., et al. (2023). Acidic pH-Triggered Release of Doxorubicin from Ligand-Decorated Polymeric Micelles Potentiates Efficacy against Cancer Cells. ACS Appl. Nano Mater. *6*, 18988–18998.
74. Weeks, J.D., Chandler, D., and Andersen, H.C. (1971). Role of repulsive forces in determining the equilibrium structure of simple liquids. J. Chem. Phys. *54*, 5237–5247.
75. Sharma, A., Kapri, R., and Chaudhuri, A. (2022). Driven translocation of a semiflexible polymer through a conical channel in the presence of attractive surface interactions. Sci. Rep. *12*, 19081.
76. Saltzman, E.J., and Muthukumar, M. (2009). Conformation and dynamics of model polymer in connected chamber-pore system. J. Chem. Phys. *131*, 214903.
77. Palyulin, V.V., Ala-Nissila, T., and Metzler, R. (2014). Polymer translocation: the first two decades and the recent diversification. Soft Matter *10*, 9016–9037.
78. Ikonen, T., Shin, J., Sung, W., and Ala-Nissila, T. (2012). Polymer translocation under time-dependent driving forces: Resonant activation induced by attractive polymer-pore interactions. J. Chem. Phys. *136*, 205104.
79. Slonkina, E., and Kolomeisky, A.B. (2003). Polymer translocation through a long nanopore. J. Chem. Phys. *118*, 7112–7118.

STAR★METHODS

KEY RESOURCES TABLE

REAGENT or RESOURCE	SOURCE	IDENTIFIER
rowheadSoftware and algorithms		
LAMMPS (2023)	LAMMPS	https://docs.lammps.org/Manual.html
PYTHON3.0	Python	https://www.python.org/
Ovito2.9	Ovito	https://www.ovito.org/

RESOURCES AVAILABILITY

Lead contact

Surya K. Ghosh (skghosh@nitw.ac.in)

Materials availability

This study did not generate new unique reagents.

Data and code availability

- All original codes available from the lead contact upon request.
- Any additional information required to reanalyze the data reported in this paper is available from the lead contact upon request.
- All other raw data are available from the lead contact upon request.

METHOD DETAILS

We studied the unforced translocation process of a flexible self-avoiding polymer in a free and crowded two-dimensional (2D) environment. The polymer of length L is represented by a space curve $\mathbf{r}(s)$ in 2D, where the parameter s goes from $s = 0$ to L, along the chemical distance or contour length of the chain. The standard two-dimensional coarse-grained bead-spring model of the polymer chain is used to represent the translocating polymer. In the discrete limit, the polymer consists of $N+1$ monomers of size σ which are connected by N Finite Extension Nonlinear Elastic (FENE) springs,

$$U_{FENE}(l_{ij}) = \begin{cases} -\frac{1}{2}kl_0^2 \ln\left(1 - \frac{l_{ij}^2}{l_0^2}\right), & \text{for } l_{ij} \leq l_0 \\ \infty, & \text{otherwise.} \end{cases} \quad \text{(Equation 22)}$$

Here k is the FENE spring constant, l_{ij} is the instantaneous separation, and l_0 is the maximum allowed length between two consecutive monomers. In the discrete picture, the i^{th} bead is represented by a 2D position vector $\mathbf{r}_i(t)$. The excluded volume interaction exclusively between the beads, crowders, and bead-crowders is modeled by a standard truncated short-range repulsive Lennard-Jones (LJ) potential, commonly known as Weeks-Chandler-Andersen (WCA) potential as[74]

$$U_{LJ}(r_{ij}) = \begin{cases} 4\epsilon\left[\left(\frac{\sigma_{ij}}{r_{ij}}\right)^{12} - \left(\frac{\sigma_{ij}}{r_{ij}}\right)^{6}\right] + \epsilon, & \text{for } r_{ij} \leq 2^{1/6}\sigma_{ij} \\ 0, & \text{otherwise.} \end{cases} \quad \text{(Equation 23)}$$

Here $r_{ij} = |\mathbf{r}_i - \mathbf{r}_j|$ is the distance between i and j particle, $\sigma_{ij} = (\sigma_i + \sigma_j)/2$ is the diameter of the effective interaction region of the interacting pairs with diameter σ_i, σ_j and ϵ is interaction strength of the potential. The use of a purely repulsive part of the LJ potential mimics a good solvent by cutting out the attractive effect. We consider a two-dimensional rectangular box separated by a repulsive wall in the middle consisting of rigid repulsive LJ particles of thickness the same as the diameter of a monomer with bead size $\sigma = 1$. The middle wall separates the box into two equal regions; the left side is referred to as *cis* while the right side is called *trans*. These two separate regions *cis* and *trans* are connected by a pore of length $w_H = \sigma$ and pore width $w_V = 1.6\sigma$ at the center of the wall.[50] Moreover, a study of the effect of box size has been done. The box has been chosen to be big enough so the polymer does not feel any effect from the box size. We have checked the effect of box size for different scaling parameters, such as translocation time, probability, and MSD (t) and our model matches with both experimental and analytical scaling regime. The geometry of the cavity plays a crucial role and has been studied extensively.[57,75–79] In our simulation, the

equation of motion of the dynamics of the i^{th} monomer is governed by the Langevin equation, by neglecting the hydrodynamic interactions, can be written as

$$\begin{aligned} m\frac{d^2\mathbf{r}_i(t)}{dt^2} &= -\xi\mathbf{v}_i(t) + \mathbf{F}_i^R(t) - \sum_{j=1, i\neq j}^{N+1} \nabla U_{LJ}\left(|\mathbf{r}_i - \mathbf{r}_j|\right) \\ &\quad - \nabla U_{FENE}(|\mathbf{r}_i - \mathbf{r}_{i\pm1}|) - \sum_{j=1}^{N_c} \nabla U_{LJ}\left(\left|\mathbf{r}_i - \mathbf{r}_j^c\right|\right) \\ &\quad - \nabla U_{LJ}(|\mathbf{r}_i - \mathbf{R}_{Wall}|) - \nabla U_{LJ}(|\mathbf{r}_i - \mathbf{R}_{Box}|), \end{aligned} \quad \text{(Equation 24)}$$

where $\mathbf{r}_i$ is the position, m is the mass, $\mathbf{v}_i$ is the velocity of the i^{th} monomer, N_c is the number of crowder, $\mathbf{r}_j^c$ is the position of the j^{th} crowding particle and ξ is the friction coefficient, and thermal fluctuation is considered by F_i^R which is the random forces satisfying the fluctuation-dissipation theorem,

$$\langle \mathbf{F}_i^R(t)\rangle = 0, \langle \mathbf{F}_i^R(t)\cdot\mathbf{F}_j^R(t')\rangle = 2dk_BT\xi\delta_{ij}\delta(t-t'), \quad \text{(Equation 25)}$$

that connect the particle diffusivity to the friction coefficient $D = k_BT/\xi$. Here d is the dimension of the system, in our case $d = 2$, k_B is the Boltzmann constant, T is the temperature, and i and j represent the coordinate components. The presence of the confining rectangular box is represented by $\mathbf{R}_{Box}(x,y)$, where $x \in [-L_x, L_x]$, $y \in [-L_y, L_y]$ and $L_x = 2L_y$. The wall in the middle is represented by $\mathbf{R}_{Wall}(x = 0, y)$ and the pore is represented by $\mathbf{R}_{pore}(x = 0, y = 0)$. Similarly, the corresponding Langevin equation[36] for the dynamics of the i^{th} crowding particle can be written, where m_i^c is the i^{th} crowding particle's mass, $r_i^c(t)$ is crowder position at time t, and other crowding particles at position $r_j^c(t)$, ξ is friction coefficient, v_i^c is the i^{th} crowder's velocity (Equation S1). The sizes of a crowder are represented as σ_c for the cis-side and σ_t for the trans-side. The friction and mass of the crowder on each side are proportional to their sizes, with $\xi_t/\sigma_t = \xi_c/\sigma_c$ and $m_t/\sigma_t^2 = m_c/\sigma_c^2$ respectively. We are using LJ parameters m, σ, ϵ for defining mass, distance, and energy scales corresponding to $t = \sqrt{m\sigma^2/\epsilon}$ and $f = \epsilon/\sigma$ for time scales and force scales in ps and pN respectively. The dimensionless parameters used in the simulation are temperature $T = 1.2$, the maximum allowed separation between each monomer $R_0 = 1.5$, spring constant $k = 30$, friction $\xi = 0.7$, the mass of each monomer $m = 1$. Values for simulation parameters used in modeling can be obtained from Table S1. For each translocation process, as a starting configuration, we placed the middle monomer $(N/2+1)$ at the center of the pore. We keep the middle monomer fixed until the rest of the polymer equilibrates for 10^5 time steps. All the simulations are performed using a Langevin thermostat, to begin with, a truly random initial configuration. The equation of motion is integrated using the velocity Verlet algorithm in each step. After the equilibration time, the middle monomer is released to allow the translocation process. After each successful translocation event, where the polymer ends up moving completely to either side of the wall, the simulation is stopped. In order to get satisfactory statistics, we averaged our data over 10^3 independent realizations, with a time step $\Delta t = 0.005$.

QUANTIFICATION AND STATISTICAL ANALYSIS

(1) Calculation of translocation probability and time in a free environment
(2) Calculation of Translocation Rate, Crossing Time and Bead Velocity
(3) Free energy calculation of an asymmetrically placed polymer in a free environment
(4) Translocation probability and time as a function of crowder size σ and their packing fraction φ in a crowded environment
(5) Effect of the asymmetrically placed polymer on translocation probability in crowded environment
(6) Effect of crowding size on translocation probability in the crowded environment